Atmospheric Research 230 (2019) 104624

Contents lists available at ScienceDirect

Atmospheric Research

journal homepage: www.elsevier.com/locate/atmosres

Invited review article

Radio occultation and ground-based GNSS products for observing, understanding and predicting extreme events: A review

Stefania Bonafoni[a], Riccardo Biondi[b,*], Hugues Brenot[c], Richard Anthes[d]

[a] Dept. of Engineering, University of Perugia, Perugia, Italy
[b] Dipartimento di Geoscienze, Università di Padova, Padova, Italy
[c] Royal Belgian Institute for Space Aeronomy (BIRA-IASB), Brussels, Belgium
[d] COSMIC Program Office, University Corporation for Atmospheric Research, CO, USA

ARTICLE INFO

Keywords:
GNSS
Ground-based
GNSS-receivers
Radio-occultation
Extreme-events
Heavy-rainfall
Convective-storms
Tropical-cyclones
Atmospheric-rivers
Droughts
Heat waves

ABSTRACT

In this paper we review the contributions of GNSS ground-based and radio occultation receivers to the understanding and prediction of severe weather phenomena around the world. These ground- and space-based GNSS observations, which are complementary to other in-situ and remotely sensed observations, are sensitive to the temperature and water vapor content of the atmosphere, both important parameters that characterize the structure and evolution of heavy rainfall and convective storms, atmospheric rivers, tropical cyclones, and droughts and heat waves. With the first ground-based GPS observations reported in the early 1990s and the first radio occultation observations of Earth's atmosphere derived from the GPS/MET proof-of-concept mission (1995–1997), these GNSS-based observations are still relatively new contributors to the research and operational suite of technologies.

1. Introduction

The Intergovernmental Panel on Climate Change (IPCC) defines (http://www.ipcc-data.org/guidelines/pages/glossary/glossary_e.html) an extreme weather event as "an event that is rare at a particular place and time of year." IPCC specifies that the definition of rare can vary, as well as how extreme weather characteristics can vary from place to place. The IPCC also extends the definition stating "When a pattern of extreme weather persists for some time, such as a season, it may be classed as an extreme climate event (e.g., drought)". Therefore, extreme weather/climate events include heavy rainfall, convective storms and tornadoes, tropical cyclones, atmospheric rivers, droughts, heat and cold waves, snowstorms and blizzards.

Owing to the risks to life, ecological systems, and infrastructure, including transportation, agriculture and communication, extreme events are of high interest to scientists and managers across different disciplines, e.g. climatology, hydrology, ecology, Earth sciences, engineering and social sciences (McPhillips et al., 2018). These impacts press scientific communities to improve the observation, understanding, and prediction of extreme weather and climate events by exploiting different instruments, analysis and modeling systems and communication methodologies. This attention is even more relevant considering that extreme events are expected to increase in intensity, frequency, and duration in the coming decades as climate continues to warm (McPhillips et al., 2018).

Recent advances in satellite remote sensing and the increasing availability of space-based atmospheric products have proved extremely valuable for studying extreme events and for developing new research approaches to observe, model, and forecast their spatial and temporal behavior. Today, detection and prediction of severe events are increasingly accurate, thanks to the timely access to reliable data from many sources, including satellites, models, and in situ measurements. Observations using the Global Navigation Satellite Systems (GNSS) radio signals have been used to study extreme events in recent years.

Abbreviations: AR, atmospheric river; CPT, coldest point tropopause; GNSS, global navigation satellite systems; GW, gravity waves; IPCC, intergovernmental panel on climate change; IWV, integrated water vapor; LEO, low earth orbit; LRT, lapse rate tropopause; NWP, numerical weather prediction; PW, precipitable water; RO, radio occultation; ROHP, radio occultation and heavy precipitation; STD, slant total delay; TC, tropical cyclone; TTL, tropical tropopause layer; TWS, terrestrial water storage; UTLS, upper troposphere-lower stratosphere; WRF, weather research and forecasting; ZHD, zenith hydrostatic delay; ZTD, zenith total delay; ZWD, zenith wet delay

* Corresponding author.
E-mail address: riccardo@biondiriccardo.it (R. Biondi).

https://doi.org/10.1016/j.atmosres.2019.104624
Received 30 April 2019; Received in revised form 5 July 2019; Accepted 14 July 2019
Available online 16 July 2019

GNSS refers to any satellite constellation used for positioning, navigation, and timing, e.g. Global Positioning System (GPS, USA), GLObal NAvigation Satellite System (GLONASS, Russia), Galileo (European Space Agency), and BeiDou (China). GNSS signals can be used to characterize the atmosphere through which they pass. The 1990s witnessed the proof-of-concept of the so-called "GPS Meteorology," using both ground-based (GB) GNSS receivers (Bevis et al., 1992) and radio occultation (RO) limb sounding (Ware et al., 1996). GPS Meteorology has provided a great boost to weather and climate studies, operational weather prediction, and space weather research and operations.

GNSS GB networks measure the tropospheric delay and the associated Integrated Water Vapor (IWV, total amount of water vapor in a vertical atmospheric column in kg/m^2) with high temporal and spatial resolution, whilst GNSS RO profiles provide valuable information on the vertical structure of Earth's atmosphere. Because GNSS signals are only slightly affected by clouds and precipitation (Solheim et al., 1999), since the early 2000's a part of "GNSS Meteorology" literature has been directed toward the investigation of extreme events where clouds and precipitation are widespread. Furthermore, this research field is the focus of several international projects. We cite the ES1206 COST action from 2013 to 2017 (Advanced Global Navigation Satellite Systems tropospheric products for monitoring Severe Weather Events and Climate, known as GNSS4SWEC), the FP7-PEOPLE-2012-IEF-CONSYDER (CONvective SYstems DEtection and analysis using Radio occultations), and the EUMETNET EIG GNSS water vapor program, which provides near-real-time GNSS delay and IWV estimates for > 1500 GNSS sites, mainly in Europe.

Both GB and RO observations provide independent temperature and water vapor (WV) information, offering unique capabilities to complement other observing systems to study the characteristics, patterns and trends of severe weather/climate events. GB GNSS observations provide accurate information on the vertically integrated water vapor at high temporal resolution that is difficult to obtain by other means. GNSS-RO provide accurate and precise vertical profiles of bending angles and refractivity (functions of temperature, water vapor and pressure) at high vertical resolution in all weather (clear-overcast) conditions that cannot be obtained by any other observation system from space. In addition, their sensitivity to WV and their accuracy and lack of significant bias makes them useful when assimilated into numerical weather prediction (NWP) models for forecasting or nowcasting of extreme events.

This study reviews GNSS contributions to studies of extreme weather and climate events. We review GNSS GB and RO methods and results, both as independent products and as contributions to NWP simulations and forecasts. We conclude with a summary of the limitations, challenges, and future directions of GNSS research on severe events.

2. Statistics of selected papers

This section reviews studies of extreme weather/climate events that used GB and RO techniques from their origin, more than 20 years ago, to the present (May 2019). Firstly, we considered the following types of severe weather: heavy rainfall, convective storms, tropical cyclones, atmospheric rivers, droughts, cold and heat waves, snowstorms and blizzards. We searched for research papers published in peer-reviewed journals in English using Web of Science and Google Scholar databases. We found 122 journal publications (all cited in the text) representative of the use of GNSS techniques for the investigation of severe events.

We grouped papers into GNSS GB (n = 74) and GNSS RO (n = 48) categories, dividing them further if extreme events are analyzed using GNSS products "stand alone" or in NWP products (Fig. 1).

The most frequent journals are J. Geophys. Res. (15 papers), Mon. Wea. Rev. (13), Atmos. Meas. Tech. (11), and Atmos. Chem. Phys. (10).

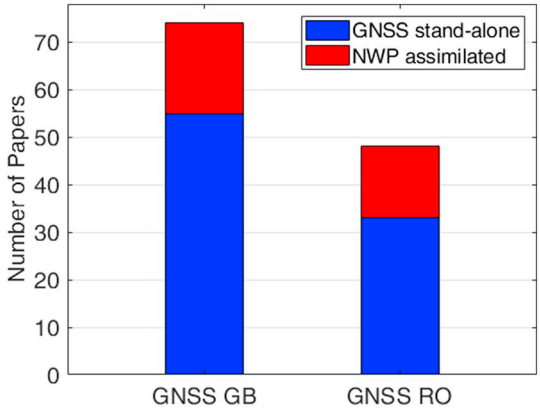

Fig. 1. Number of reviewed papers and their categorization (GB = ground-based receivers; RO = radio occultation limb sounding).

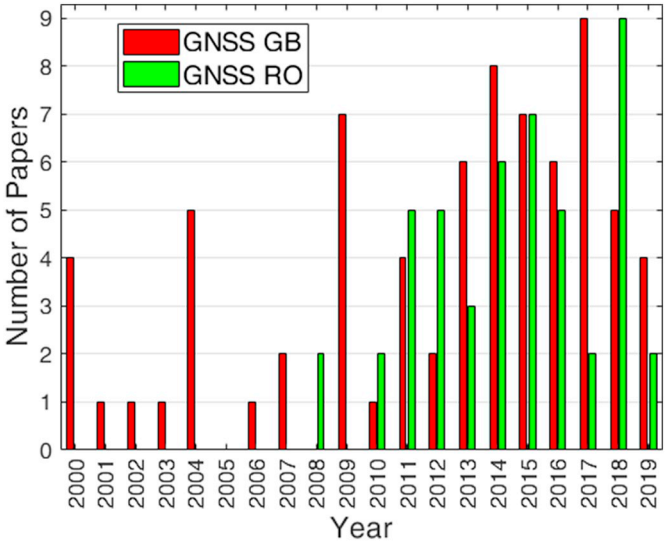

Fig. 2. Number of reviewed papers across the years; the year 2019 considers only the first six months.

2.1. Temporal trend

The interest in extreme event analysis by using GNSS signals is reflected in the literature starting from the year 2000 (Fig. 2).

From 2000 to 2007, we found only journal papers employing observations from GNSS ground-based receivers; the yearly number of GB papers reached a peak in 2017. Conversely, papers using the RO limb sounding technique to study severe weather appeared later (following the COSMIC launch in 2006), with the first papers on atmospheric rivers and tropical cyclones appearing in 2008.

2.2. Extreme weather/climate events investigated

From the standpoint of the event type, the GNSS research papers are distributed as shown in Fig. 3.

The most frequently examined extreme events are weather-related: the top three are convective storms, tropical cyclones, and heavy rainfall. There are still no papers dealing with cold waves, snowstorms and blizzards. Event considering GNSS GB and GNSS RO separately are shown in Table 1.

2.3. Geographic patterns

The geographic areas of the extreme events studied by GNSS

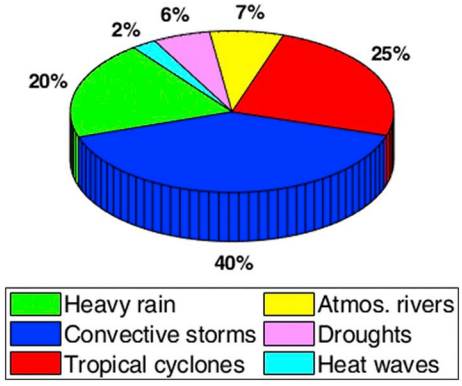

Fig. 3. Percent of all GNSS papers investigating different extreme weather/climate events.

encompass all continents and oceans, with Europe, Asia and oceanic regions having the greatest representation (Fig. 4a). Only one paper focused on Africa. Fig. 4b shows the extreme event distribution among the oceans, for a total of 29 papers, with almost all studying tropical cyclones.

3. GNSS ground-based results

3.1. Basics of GNSS GB technique

The GNSS GB technique uses GNSS signals received by instrumentation situated at the Earth's surface. Equipped with a geodetic antenna, each station records signals emitted by the GNSS constellation. Combined with the adjustment of precise positioning solutions, retrieving tropospheric parameters requires a precise quantification of signal phase delay (Teunissen et al., 1998). Using records of precise phase variations of the GNSS signals for two L-band wavelengths, a correction for the ionospheric delay is applied by using the ionospheric-free combination (Klobuchar, 1996) to focus only on the specific delay of the neutral atmosphere.

The signal processing requires the adjustment of clock parameters, the resolution of ambiguities of GNSS signals, the detection of carrier cycle-slips and a quality check of data records, the characterization of the antenna pattern and multipath effect, and the input of precise trajectories of GNSS satellites (Lichten and Border, 1987; Blewitt, 1989).

Two types of tropospheric parameters are retrieved by GNSS Meteorology. The first describes the mean state of the neutral atmosphere above a GNSS station during a selected time window (generally from 5 to 30 min). The mean Zenith Total Delay (ZTD) of the neutral atmosphere and the mean horizontal delay gradients (north-south and an east-west components) belong to this first type. The second type is a direct measurement of the state of the troposphere in the direction of the GNSS satellites, e.g. the Slant Total Delay (STD) of the neutral atmosphere; the time resolution of STD can range from 1 to 30 s.

With the assumption of an atmosphere in hydrostatic equilibrium, it is possible to estimate the IWV from the ZTD by its decomposition into the Zenith hydrostatic Delay (ZHD), dependent on the atmospheric dry air gasses (Saastamoinen, 1972; Bonafoni and Mattioli, 2018), and the Zenith Wet Delay (ZWD), dependent on the tropospheric WV content. Then, it is possible to convert ZWD into IWV by the following relationship:

$$IWV = \Pi \cdot ZWD \quad (1)$$

where Π (Fig. 5) is a function of physical constants and of the weighted mean temperature of the atmosphere (Bevis et al., 1992, 1994).

International networks, systems, associations and services, like the Global Geodetic Observing System (GGOS), the International Association of Geodesy (IAG), and the International GNSS Service (IGS), provide satellite and tropospheric products that are essential for the development and use of GNSS Meteorology.

Tropospheric GNSS GB products can be retrieved using different geodetic software: GAMIT developed by the MIT (Massachusetts Institute of Technology), BERNESE developed by the AIUB (Astronomisches Institut der Universität Bern), GIPSY-OASIS developed by JPL (Jet Propulsion Laboratory), EPOS developed by GFZ (German Research Centre for Geosciences), G-Nut/Tefnu developed by GOP (Geodetic Observatory Pecny), and NAPEOS developed by ESA (European Space Agency). Rohm et al. (2014) investigated a number of GNSS signal processing techniques using a selection of IGS orbit and clock products for severe convective weather events involving flooding and found that the ZTD and IWV estimates from a double-differenced network solution were the most reliable, with very small biases and errors.

3.2. Observing extreme events using GNSS GB products

Table 1 shows that the most frequently examined extreme events by GNSS GB technique are convective storms and heavy rainfall. The following sub-sections review results using GNSS GB products for each event category.

3.2.1. Heavy rainfall

Heavy rainfall is one of the most widespread and frequent severe weather phenomena, often leading to flooding and landslides. In this section, we have selected papers dealing with heavy rain events that do not specify if they are associated with convective systems; the latter will be considered in the Section 3.2.2.

The study of the temporal variation of IWV before and after the onset of precipitation has been the main target of the literature dealing with heavy rainfall phenomena. The first paper published by Iwabuchi et al. (2000) analyzed the trend of IWV time series estimated from several GNSS sites during a heavy frontal rainfall event in Japan. Temporal anomalies of IWV from average values were detected moving along the front. After the front moved away, IWV decreased rapidly. A common finding from the literature is an increase in IWV reaching a peak just before the start of the precipitation (Van Baelen and Penide, 2009; Li and Deng, 2013; Priego et al., 2017; Sapucci et al., 2018). This characteristic is clearly shown in Fig. 6 for three stations in Spain (Priego et al., 2017).

After the peak, the total WV varies in different ways: Li and Deng (2013) found that rainfall occurred mainly during high levels of WV, but highlighted differences in the IWV evolution caused by different weather systems. Huelsing et al. (2017) showed that IWV remained quite constant for the entire flood event analyzed, a result of a nearly

Table 1
Extreme events partitioning GNSS GB/RO. The value refers to the number of papers (numbers without brackets represent all GNSS papers, in brackets the GNSS NWP products).

	Heavy rain	Convective storms	Tropical cyclones	Atmospheric rivers	Droughts	Heat waves
GNSS GB	6 (7)	37 (12)	5 (0)	6 (0)	7 (0)	3 (0)
GNSS RO	8 (3)	12 (1)	25 (9)	3 (2)	0 (0)	0 (0)

The most frequently analyzed events in the GNSS GB literature are convective storms and heavy rains; the lack of ground-based receivers over ocean surfaces limits their use in tropical cyclone studies. Conversely, tropical cyclones are the most examined phenomenon by GNSS RO.

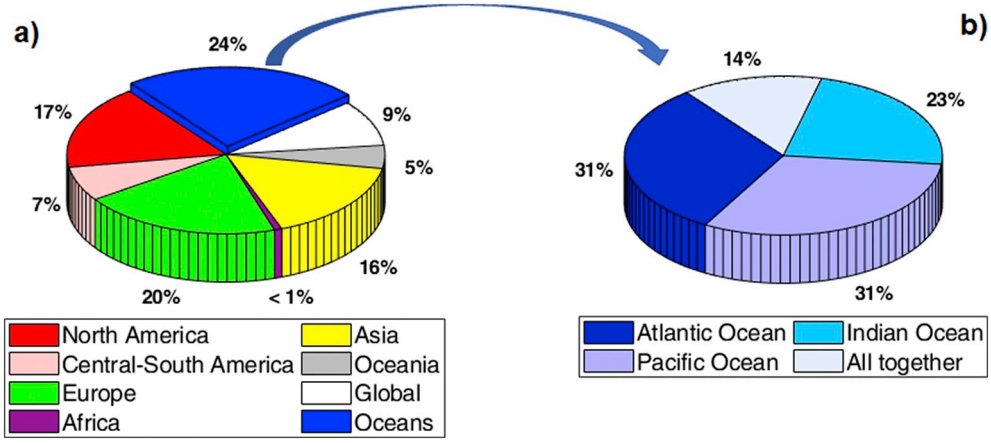

Fig. 4. a) Geographic distribution of the selected GNSS literature based on event location. b) Distribution of the events, almost all tropical cyclones, over oceans (28 papers by GNSS RO).

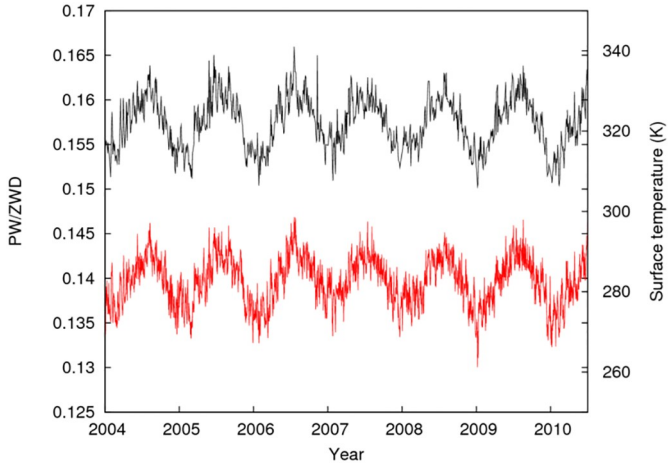

Fig. 5. Values of ratio of precipitable water (PW in mm) to ZWD (in mm), shown in black line, and surface temperature (red line) from seven years of radiosonde data from Uccle, Belgium. ZWD is given in units of equivalent excess path length and PW = IWV times the density of water. (For interpretation of the references to colour in this figure legend, the reader is referred to the web version of this article.)

saturated atmosphere that remained even after the heavy precipitation ended. Barindelli et al. (2018) found a steep decrease of IWV after the rainfall. Sapucci et al. (2018) found a short period of decreasing IWV just before the onset of strong precipitation. A possible reason for this decrease is the conversion from water vapor to liquid. Despite the typical increase/decrease trend of IWV before/after the heavy rain event, these studies indicate that the relationship between rainfall intensity and IWV varies for each precipitation event, as well as the time interval between the occurrence of the IWV peak and precipitation maximum; however, the increase in WV prior to the onset of heavy rain is well documented for all cases.

The observed increase in IWV before the onset of precipitation has encouraged researchers to establish warning systems for heavy rainfall. The identification of IWV thresholds inferred from analyses of IWV trends just before the onset of strong rainfall events can be used for rainfall recognition, and their use together with surface meteorological parameters is promising (Sharifi et al., 2015; Benevides et al., 2019). For instance, a rise in IWV combined with a drop in atmospheric pressure is a common precursor to heavy rainfall (Priego et al., 2017).

GNSS networks with stations at different altitudes can provide useful information about the IWV vertical variability in the lower part of the atmosphere during heavy rainfall. A study carried out by Van Baelen and Penide, 2009 for a short but intense rain episode exhibited a nearly constant WV content in the near surface atmospheric layer, while more significant WV variations arose in the upper levels over a mountain top (about 1500 m). The median layer, between these lower and upper levels, exhibited a relatively constant WV content.

GNSS GB products have proven useful in NWP model forecasts of heavy rainfall events. Assimilation of ZTD was tested in different models (e.g. Weather Research and Forecasting (WRF), Fifth-Generation Mesoscale Model (MM5), High Resolution Local Area Modeling (HIRLAM)), mainly using four-Dimensional Variational assimilation (4D-VAR) systems.

A positive impact of ZTD assimilation on short-range precipitation forecasts was assessed for different events (De Pondeca and Zou, 2001; Vedel et al., 2004), as well as on the correction of rainfall underestimation of strong events (Poli et al., 2007). The beneficial impact of assimilating GNSS ZTD in NWP models for quantitative precipitation forecasting can be further improved using larger and denser GNSS networks (Bauer et al., 2011). In addition to the improvements in GNSS ground infrastructures, preprocessing techniques expressly developed for ZTD observations before the assimilation (Poli et al., 2007), as well as an enhanced description of its background error statistics (Lindskog et al., 2017), are methodological aspects to consider for better heavy rainfall forecasts.

In the case of heavy rainfall leading to flash flooding, the assimilation of IWV data at intervals between 1–6 h to detect rapid moisture increases can contribute to timely flood detection and warning (Moore et al., 2015). Recently, the assimilation into the WRF model of a 3D WV pattern retrieved by means of GNSS tomography during a heavy rainfall event improved the retrieval of the wet refractivity (Xiong et al., 2019).

These results show how dense GB networks, near-real-time data with high temporal resolution and accuracy are key-points for a beneficial contribution of GNSS data into NWP for extreme rainfall forecasting.

3.2.2. *Convective storms*

Convective storms (thunderstorms) are responsible for lightning, hail, heavy precipitation, strong winds, tornadoes and waterspouts. Often these storms are organized into squall lines or mesoscale convective systems, or into long-lived supercells.

3.2.2.1. Convective systems and IWV variations. Several papers have investigated the relationship between convective precipitation and GNSS-IWV variation, with the objective of understanding the life cycle of convective storms and finding precursors of these extreme events. The high temporal and spatial resolution of GB networks allows for an unprecedented 2D or 3D view of the changes in WV during all

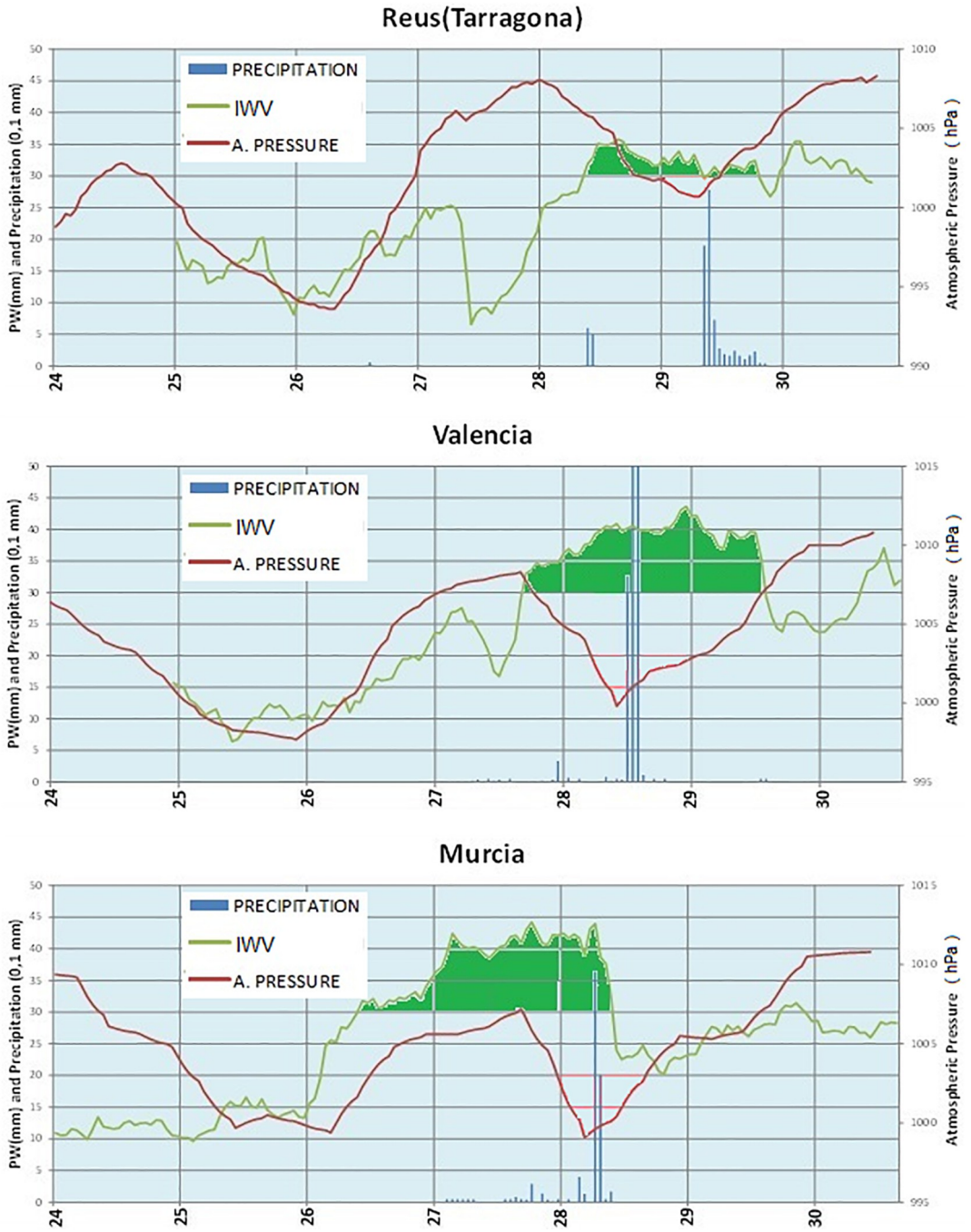

Fig. 6. Time series from 24 to 31 July 2012 of precipitable water (left ordinate in mm, light green line), pressure (right ordinate in hPa, red line) and precipitation (left ordinate in 0.1 mm, blue bars) at three locations in Spain. Precipitable water > 30 mm is shaded in solid green. (Source: Fig. 5 from Priego et al., 2017). (For interpretation of the references to colour in this figure legend, the reader is referred to the web version of this article.)

stages of the convective systems, before and after the onset of severe weather (Seko et al., 2000; Ha et al., 2002; Champollion et al., 2004; Seko et al., 2004).

If the GB GNSS network is dense enough, a three-dimensional analysis of the WV field can be obtained through tomographic techniques. Van Baelen et al. (2011) constructed 3D analyses of WV for several case studies of heavy precipitation in the Rhine Valley in 2007. Using a network of GNSS receivers with an average separation of under 40 km, the 3D water vapor field was constructed on a 16-km horizontal grid. Fig. 7 shows one such analysis for the 1000 m level at 13UTC 12 August 2007 and Fig. 8 shows a vertical west-east cross section of WV at latitude 48.1875 N (lower dashed line in Fig. 7). This study showed that the accumulation of WV on the crest of ridges was a precursor to local convective cell generation, as well as other complex relationships between the terrain and large-scale flow.

Other studies have used tomography to monitor the spatial and temporal correlation between IWV variations and the formation and passage of the storms. For example, Champollion et al. (2009) showed that the GPS data from a mesoscale network in the central U.S. clearly added value to the analysis of the horizontal and vertical structure of water vapor compared to the use of radiosonde data alone. Similarly, Manning et al. (2012), Choy et al. (2013) and Zhang et al. (2015) showed the additional value of GPS data by providing continuous observations during the passage of convective storm systems in Australia.

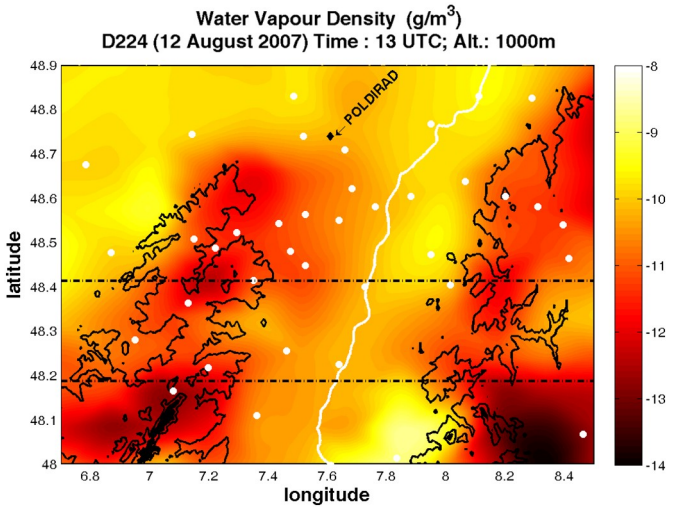

Fig. 7. Horizontal water vapor density fields for 1000 m height level at 13UTC 12 August 2004 over the Rhine valley and Black Forest hills obtained by GPS tomography. The water vapor density field ranges from 8 (light colors) to 14 g/m^3. The white dots show the position of the GPS stations, the POLDIRAD show the position of the weather radar, the horizontal dashed lines indicate the vertical cross-sections reported in Fig. 8, and the black lines are the 500 m height contours of the terrain. Longitude and latitude are in degrees. (Source: from Fig. 11 of Van Baelen et al., 2011).

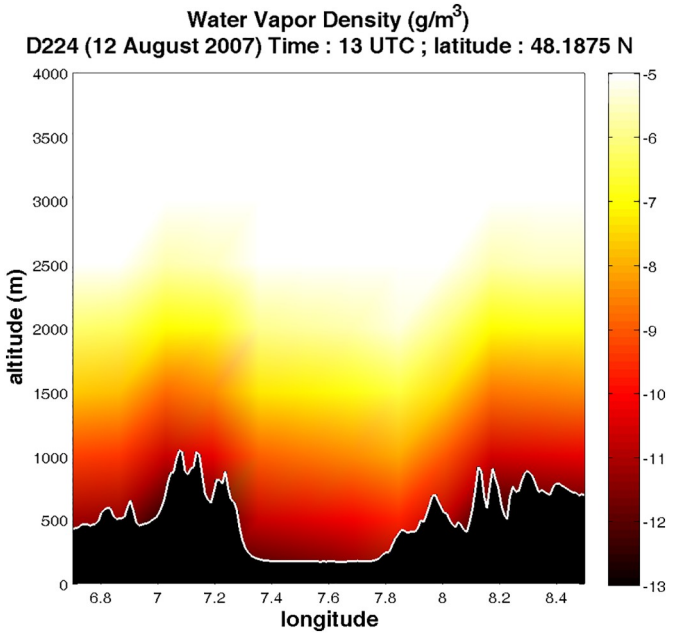

Fig. 8. Vertical WV density cross section at latitude 48.41 N at 13UTC 12 August 2007 (lower dashed line in Fig. 7). WV density scale ranges for 5 g/m^3 (light colour)–13 g/m^3 (dark colour). Longitude and latitude are in degrees. (Source: from Fig. 12 of Van Baelen et al., 2011).

Additional results for convective storms in southeastern France are presented by Brenot et al. (2014). Recently, a study of a convective supercell storm cross-validated different tomography models (Brenot et al., 2018), suggesting that the best approach is the use of an ensemble tomography solution. Guerova et al. (2016) review the tomographic inversion technique and point out that an improvement in the tomography performance depends on the density of GNSS stations and accuracy of the inversion techniques.

A 3D analysis of the WV field using GNSS-STD observations highlighted the height extension of the moist air in the early stage of convective events and during thunderstorm formation, as well as dry air intrusion at a later stage of the convective system (Seko et al., 2000; Seko et al., 2004). Besides the significant increases in IWV prior to the storm and precipitation extreme (Zhang et al., 2015), the evolving moisture pattern can show unstable structures and local motion strongly related with the development and maintenance of precipitation (Wang et al., 2015).

In addition to 3D views of WV, the computation of GNSS horizontal wet gradients also helps describe the anisotropy of the IWV field during the passage and evolution of convective systems (Champollion et al., 2004). GNSS horizontal delay gradients can also detect small-scale convective structures (Brenot et al., 2013).

Another parameter useful for the analysis of the life cycle of convective events is WV convergence. Severe storms are often preceded by low-level moisture convergence, and the time tendency of IWV provides an estimate for WV convergence that can be also used to predict rainfall associated with convective systems (Banacos and Schultz, 2005). Using GNSS GB products, de Haan et al., 2009 showed that moisture convergence is associated with the location of developing thunderstorms. Near-real-time IWV maps highlighted areas with strong WV convergence that triggered convection, as in so-called air-mass thunderstorms (Terradellas and Téllez, 2010; Graham et al., 2012).

3.2.2.2. Convective systems in continental tropical regime. Several studies have analyzed convection systems over the Amazon region by using data from the Amazon Dense GNSS Meteorological Network (ADGMN), which was created to study water vapor–convection interactions. Such networks, with average distance between receivers ranging from 5 to 10 km, have proved useful 1) for tracking WV advection and identifying WV convergence time scales, i.e. the time scale of local increase and change of IWV and 2) for improving the understanding of the complex interaction on the mesoscale between WV field and shallow-to-deep convection transition. Adams et al. (2011, 2013, 2015) analyzed IWV time-series for hundreds of deep precipitating convective events to infer the WV convergence time scale, a useful metric for examining the temporal evolution of deep convection. A 4-h WV convergence time scale indicative of the shallow-to-deep transition for continental tropical convection proved robust regardless of intensity, seasonality, and daytime of convective event. Also, a spatial correlation decay time scale of about 3.5 h during the evolution of a deep convection was found, which is very close to the above WV convergence time-scale (Adams et al., 2017). The transition from shallow to deep convection and the diurnal cycle of precipitation in tropical regions were also investigated using high-frequency (5 min) GNSS GB retrievals. Adams et al. (2015) showed that WV convergence is generally less intense during the wet season, with strong evidence of local topographic effects.

3.2.2.3. New techniques for estimating IWV and ZTD. Some studies have focused on new procedures for estimating the IWV distribution in the environment of convective storms, and their reliability tested on convective storm cases. Shoji et al. (2014) estimated IWV gradients in each GNSS-STD direction by computing the difference between ZTD and zenith-mapped STD, assuming an exponential distribution for the horizontal WV gradient. A study of a tornado showed strong small-scale WV variations. Shoji et al. (2015) demonstrated the accuracy of this new procedure for detection of severe convection. Simulations showed that dense GNSS stations (15 km spacing) can detect local moisture variations associated with convection that the conventional methods for IWV estimation do not capture.

Another new technique for retrieving WV and its geographical distribution considers the mapping of IWV using a digital model of terrain (Calori et al., 2016). They tested this method during intense convective events and found a high correlation between the accumulation/depletion of atmospheric moisture and hail/no hail precipitation. However, at some locations, as a consequence of strong atmospheric gradients,

GNSS-IWV estimates were unrealistic.

Masoumi et al. (2017) proposed a new directional model for the computation of the horizontal delay gradient in the troposphere. Compared with the conventional planar model during an extreme convective event, the proposed directional model provided a more accurate pattern of the horizontal delay gradients.

3.2.2.4. Assimilation of GNSS GB data in NWP models. Different papers have evaluated the impact of assimilating GNSS GB products in NWP models (e.g. MM5, WRF, Meso-NH, AROME) for convective storm prediction. These studies use different methods of data assimilation, e.g. three- and four-dimensional variational (3D-VAR and 4D-VAR) methods. The general benefit of assimilating GNSS ZTD is to improve the moisture analysis in the low-to-middle troposphere, as pointed out in different cases of convection forecasts in which spatial extent and intensity of precipitation were estimated (Cucurull et al., 2004; Brenot et al., 2006; Yan et al., 2009a; Yan et al., 2009b; Boniface et al., 2009). However, the positive impact of assimilating ZTD data is case-dependent and likely dependent on the method of data assimilation. Situations in which the model analysis of water vapor is already good show little impact of assimilating additional ZTD observations (Boniface et al., 2009; Peng and Zou, 2004).

The impact of assimilating GNSS-IWV alone or with other observations in NWP models has been studied for convective events (Serra et al., 2016; Moker Jr et al., 2018; Guo et al., 2000; Zhang et al., 2007; Kawabata et al., 2014; Rohm et al., 2019). The main and common finding is that the assimilation of the IWV in NWP models improves the precipitation forecast skill. As with the assimilation of ZTD data, when combined with different data, the impact of the IWV observations varies with the case studied. For instance, Guo et al. (2000) assimilated GNSS-IWV in MM5, along with wind profiler, hourly rainfall, and surface dewpoint data. The IWV data improved the prediction of rainfall for a squall line, but had little influence on the analysis of the vertical structure of humidity, for which wind profiler and dewpoint data had maximum impact. Zhang et al. (2007) confirmed the positive impact GNSS-IWV on a short-range prediction of precipitation for a mesoscale convective system. They also indicated that assimilation of rainfall observations requires careful selection of observation weights and control of spurious gravity waves.

Kawabata et al. (2014) assimilated different data (wind measurements, radar reflectivity, and GNSS-IWV) in NWP models to monitor a mesoscale convective system. Results showed that the effect of the assimilation was minor when the observations were considered separately, but their combination yielded a notable improvement in forecasts of the convection and the associated precipitation. Rohm et al. (2019), investigating three convective storms, found that IWV assimilation alone improved the rain prediction, but that an improvement of the vertical distribution of humidity was obtained by assimilating IWV with surface synoptic observations.

3.2.3. Tropical cyclones

Tropical cyclones (TC) are intense rotating storm systems, characterized by strong winds, heavy rains and storm surges, that originate over warm tropical oceans. Since GNSS GB products over oceans are only sporadically available (receivers installed on ships, buoys or islands), the few GB GNSS papers on TC have used coastal receivers.

The analyses of the temporal trend of IWV retrieved by GNSS GB stations during TC occurrences show the same behavior: an increase of IWV as the TC approaches and a quick decrease after the TC passage. Liou and Huang (2000) estimated an increase/decrease of about 3/5 cm for Typhoon Zeb 1998 in Taiwan (Fig. 9). The IWV increases until the typhoon passes, then rapidly decreases. The GNSS GB estimates agree well with the Taipei radiosonde (banc site).

Song and Grejner-Brzezinska (2009), using a network of GNSS GB stations in South Korea, confirmed the increase of IWV before the passage of the typhoon Ewiniar 2006, and a rapid decrease after that,

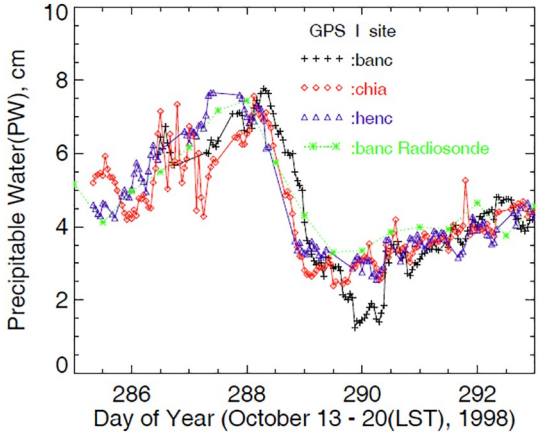

Fig. 9. Ground-based GNSS observed precipitable water (PW) at three sites (banc, chia, henc) in Taiwan and radiosonde measurements (green *) of PW at the Taipei site (banc) for 13–20 October 1998. (Source: Fig. 4 from Liou and Huang, 2000). (For interpretation of the references to colour in this figure legend, the reader is referred to the web version of this article.)

recovering to its nominal values in about one day. Seco et al. (2009) analyzed the strong tropical storm Delta Peng and Zou, 2004, a late-season TC of the 2005 Atlantic hurricane season moving toward Africa and found similar results. They used as reference the ZTD and ZWD of four GNSS stations placed in the Canary Islands and in Morocco.

In addition to the showing the temporal trend of IWV during the TC life cycle, other studies have focused on the spatial distribution of tropospheric delays and humidity values in the TC area by using dense GNSS networks (mean separation of site of~5 km). Iwabuchi et al. (2003) showed that ZTD horizontal gradients pointed toward the centre of a TC that crossed Japan, demonstrating that the tropospheric delay gradients could reveal the horizontally anisotropic distribution of water vapor in the TC. Chen et al. (2017), applying tomographic solutions during the passage of Typhoon Chanthu 2010 over the South China Sea, found that the humidity of the layer from 3 to 5 km had larger fluctuations than in the lower layer.

Overall, the retrieved WV fields during the passage of TC highlight a rapid increase followed by a decrease, a typical behaviour found during the evolution of other heavy precipitation events.

3.2.4. Atmospheric rivers

Atmospheric Rivers (AR) are long and narrow corridors of intense WV transport in middle latitudes. The large amounts of WV and the associated strong winds can cause extreme precipitation events and severe flooding. Ralph et al. (2011) studied the thermodynamic and kinematic structures of AR by multiscale analyses using a synergy of different instruments, e.g. scanning and profiling Doppler radars, GNSS GB, dropsondes, and rawinsondes. As in many studies, the GB GNSS complemented the other observing systems by showing very high-resolution time series of IWV. Several papers have studied the interactions between barrier jets and AR in California (Neiman et al., 2013; Neiman et al., 2016). The IWV temporal trend for these cases revealed increasing WV during the 12-h period preceding the arrival of the barrier jet core, with a broad peak exceeding the 2-cm minimum threshold for AR conditions. Some hours later, an IWV decrease highlighted a tropospheric drying. A similar increase in IWV beyond the 2-cm threshold was previously found in Northwestern Pacific by Ralph et al. (2011). GNSS-IWV time series combined with wind speed measurements from wind profilers can also be used to compute the IWV flux in AR (Kingsmill et al., 2013; Neiman et al., 2014). An innovative study of Wang et al. (2019) used GNSS ZTD to retrieve the arrival time of 3 AR in California in January 2017. The results show that dense GNSS networks can capture the AR movement with high spatial and temporal resolution, and that the local topography affects the movement of

landfalling AR.

3.2.5. Droughts

Droughts are natural disasters characterized by a prolonged period of dryness and very low precipitation. A drought can last for months or years and have a major impact on the agriculture and local economy of the affected area, as well as on the increase of fire probability. The monitoring of the hydrological cycle during such event is therefore of great interest.

By using GNSS GB observations of surface displacements, the temporal and spatial Terrestrial Water Storage (TWS) variations can be inferred (Borsa et al., 2014; Chew and Small, 2014). In fact, the water mass loss during drought events causes vertical and horizontal displacements that can be measured by GNSS at the millimeter level. Such loading response measured from daily vertical positions by continuous GNSS stations is used to directly quantify the water deficit (Argus et al., 2017). Borsa et al. (2014) found that the drought in March 2014 in the Western United States produced a deficit of 240 gigatons of water, equivalent to a uniform 10-cm layer of water over the entire region, equivalent to the annual mass loss of the Greenland Ice Sheet. The evaluation of TWS anomalies by GNSS vertical positions is also useful when TWS deficit persists for more time due to depleted groundwater storage, even though standard drought indices point out a more rapid recovery after the end of the most severe meteorological conditions (Chew and Small, 2014). TWS depletion caused by severe droughts and measured using GNSS data can be used to validate and improve the results of hydrological models (Fu et al., 2015; Jin and Zhang, 2016). In addition, the combination of IWV and vertical crustal displacement (VCD), both observed by GNSS stations, can be used to explore drought evolution, since VCD is in phase with equivalent water height, and IWV with precipitation (Jiang et al., 2017; Ferreira et al., 2018).

These studies demonstrate that GNSS GB products (surface displacements and IWV) can provide information useful for drought monitoring and water deficit quantification, as well as for the current hydrological observing networks.

3.2.6. Heat waves

Heat waves are prolonged periods of very high air and surface temperatures relative to the expected mean values for the season. The abnormally high temperature pattern can affect an area from several days to several weeks, with implications for human comfort and health, energy management, agriculture production, and ecosystem function. Heat waves can occur with high humidity, leading to additional harmful health effects, or by low humidity and droughts.

Few papers have studied this type of event using GNSS techniques, and they focus mainly on the WV anomalies with respect to climatological mean values. Guerova et al. (2014) and Mircheva et al. (2017) studied the long- and short-term variations of IWV from GNSS datasets over Bulgaria during the July 2007 heat wave, and showed a large negative departure of IWV (drying) from the 2001–2007 mean. Venkat Ratnam et al. (2016a) analyzed the IWV variations during a 2015 heatwave in South India, comparing the WV patterns during the event with respect to the ones two months before.

The case studies are too few to draw general interpretations; therefore, it would be interesting in the future to focus on the detection of IWV anomalies as well as on the production of 2D/3D moisture fields during heat waves to infer recurrent descriptive features.

4. GNSS RO results

4.1. Basic theory of GNSS RO technique and assimilation in NWP models

The GNSS RO technique uses L-band radio signals received on board of Low Earth Orbit (LEO) satellites after their propagation through Earth's atmosphere to measure the vertical refractivity gradient. By measuring the signal phase delay, the atmosphere can be characterized by vertical profiles of the bending angles of signal trajectories in the ionosphere, stratosphere and troposphere (Kursinski et al., 1997).

After the ionospheric correction by using the two L1 and L2 frequency measurements, bending angles and atmospheric refractivity profiles N can be obtained. At microwave wavelengths, in the stratosphere and troposphere, N is a function of temperature, pressure and water vapor (Smith and Weintraub, 1953).

$$N = 77.\,6P/T + 3.73 \times 10^5\, e/T^2 \quad (2)$$

where P is pressure (hPa), T is temperature (K), and e is the partial pressure of WV (hPa). Then, P_w, P_d, and T profiles can be retrieved from the observed N using ancillary information from sources such as operational weather analyses or short-term forecasts in order to resolve the wet-dry ambiguity information inherent in refractivity.

RO vertical resolution varies from tens of meters in the troposphere to 1 km in the stratosphere (Gorbunov et al., 2004; Zeng et al., 2019), with the greatest accuracy between 5 and 25 km altitude. The RO horizontal resolution (more properly termed footprint or horizontal scale of a single observation) is 200–300 km, with most of the information in a single profile representing an average over about 50 km (Melbourne et al., 1994). Anthes et al. (2000) discuss limitations and advantages of the vertical and horizontal spatial scales (footprint) of RO observations.

Between 2001 and 2015, almost 10 million profiles were collected by eleven different missions: GPS/MET, the CHAllenging Minisatellite Payload (CHAMP) satellite, the Satellite de Aplicaciones Cientificas-C (SA-C) satellite, the Constellation Observing System for Meteorology, Ionosphere and Climate (COSMIC) six-satellite constellation, the Gravity Recovery And Climate Experiment A/B (GRACE-A/B), the Meteorological Operational Satellites (Metop-A/B), the Communications/Navigation Outage Forecasting System (C/NOFS) satellite, TerraSAR-X and Fengyun-3C. RO data are available from six processing centers: the Danish Meteorological Institute (DMI) Copenhagen, Denmark, EUMETSAT (EUM) Darmstadt, Germany, the German Research Centre for Geosciences (GFZ) Potsdam, Germany, the Jet Propulsion Laboratory (JPL) Pasadena, CA, USA, the University Corporation for Atmospheric Research (UCAR) Boulder, CO, USA and the Wegener Center/University of Graz (WEGC), Graz, Austria.

As discussed above, RO observations provide vertical profiles of phase delays, bending angles, and refractivity. Because of their high vertical resolution, ability to sound the atmosphere over land and water and in all-sky (clear to overcast) conditions, high precision and accuracy, RO data have been shown to be very useful in global and regional numerical weather prediction (NWP). Ho et al. (2019) review the assimilation of RO in these models and compare the assimilation of phase delays, bending angles and refractivity. One of the main advantages of assimilating RO data in NWP models is that they can be assimilated without bias corrections, and hence they act as “anchors” to models to keep the models from drifting toward their own “climates.” They also act to improve the effects of infrared and microwave sounders, which typically have biases.

4.2. Observing extreme events using GNSS RO products

The most frequently examined types of extreme events by the RO technique are weather-related: tropical cyclones, convective storm and heavy rainfall (Table 1).

4.2.1. Heavy rainfall

GNSS RO can be used to quantify the rainfall rate in heavy rainfall systems. Cardellach et al. (2015, 2018) introduced the concept of dual polarization (separation of the vertical and horizontal orientations of the electromagnetic field with respect to receiving antenna) RO to detect and quantify the rain rate of heavy precipitation events. The Radio Occultation and Heavy Precipitation (ROHP) experiment on the Spanish PAZ satellite, launched 22 February 2018, is able to detect

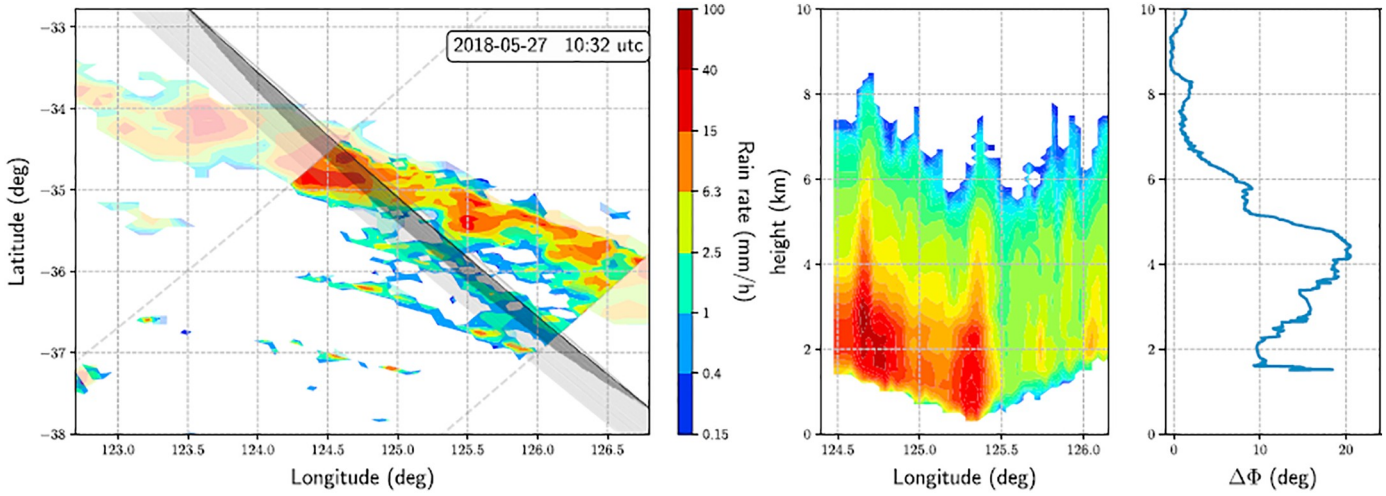

Fig. 10. Left: ROHP-PAZ path superimposed on GPM (Global Precipitation Measurement) precipitation. Middle: vertical precipitation structure from GPM interpolated to plane of ROHP-PAZ observational plane. Right: vertical profile of Δϕ (phase delay difference of horizontal and vertical polarized signals) measured by ROHP-PAZ. The Δϕ profile shows relatively large values where the GPM radar observes precipitation. (Source: Fig. 1 from Cardellach et al., 2019).

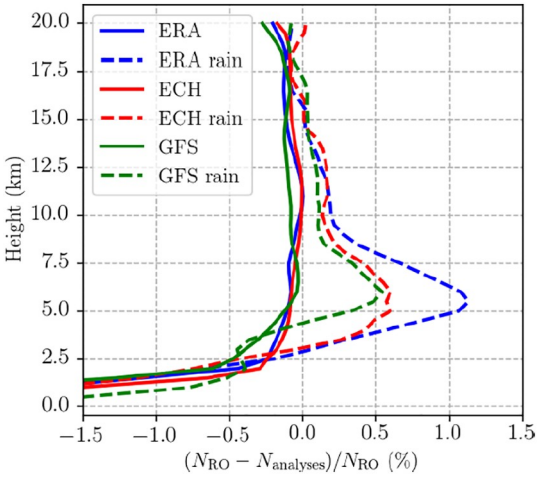

Fig. 11. Fractional difference between the RO-observed refractivity and that from ERA-Interim (blue), ECMWF high-resolution analysis (red), NCEP GFS operational analysis (green) over the region from 60°S to 60°N for 2016. The COSMIC RO profiles are divided into no rain (solid) and heavy rain (dashed). (Source: Fig. 2 from Padullés et al., 2018). (For interpretation of the references to colour in this figure legend, the reader is referred to the web version of this article.)

rainfall rates higher than 5 mm/h by using an inversion procedure from polarimetric RO to rain rate estimations. The first measurements and results obtained with the ROHP-PAZ sensor are shown in Fig. 10 (Cardellach et al., 2019).

A recent comparison of RO refractivity with three models (ECMWF, ERA-Interim and GFS) in heavy rainfall by Padullés et al. (2018) shows a positive RO refractivity bias compared to models in the mid troposphere (Fig. 11). By showing that the neglect of the effect of liquid and ice content terms in the full equation for refractivity was negligible in the calculation of RO refractivity, they showed that the three models all have a dry bias in precipitating clouds. This dry bias is caused by misrepresentation of the moist thermodynamics (de la Torre-Juárez et al., 2018).

RO refractivities and bending angles have been assimilated in WRF models to predict heavy rainfall (Ha et al., 2014; Yang et al., 2014; Huang et al., 2016), resulting in significant improvements of the forecasts, with cycling assimilation providing a better prediction of rainfall amount and location (Ha et al., 2014). The assimilation of bending angles was more effective than refractivity in deepening moist layers (Yang et al., 2014).

4.2.2. Convective storms

Several studies based on GNSS RO focus on severe convective storms. The first work on this topic validated WRF simulations of three deep convection events in Argentina by using RO temperature profiles (de la Torre et al., 2011). They found that updrafts generated by mountain waves were possible triggering mechanisms of the initiation of convective storms.

The thermal structure of convective systems can be inferred from RO temperature profiles (Biondi et al., 2012; Bonafoni and Biondi, 2016). The profiles generally show a relative temperature minimum corresponding to the cloud top and a strong inversion above, approaching the climatological temperature profile at higher altitudes. These results were achieved by using the co-location of > 2000 RO profiles with the ISCCP Deep Convection Tracking Database and validated with the Infrared Pathfinder Satellite Observation (CALIPSO) satellite observations (Biondi et al., 2012). In general, deeper convection produces larger temperature anomalies (Johnston et al., 2018), with a narrower cool layer (14–17 km) for maritime convection against a larger one (14–22 km) for land convection. Deep convection also has an important impact on the tropopause altitude and the Tropical *Tropopause* Layer (TTL).

The signature of convection is persistent in the TTL with amplitude and duration depending on the time of day (Khaykin et al., 2013) and the season (Paulik and Birner, 2012). Using six years of COSMIC RO data, Khaykin et al. (2013) found a strong diurnal temperature cycle over land in the tropics (25°S–25°N), with cooling in the lower stratosphere in phase with the maximum overshooting frequency in the afternoon. The convection associated with tropical cyclones can also generate propagating gravity waves (GW, Hierro et al., 2018). RO profiles combined with other measurements, such as the Tropical Rainfall Measuring Mission (TRMM) precipitation radar, were used to assess the probability of deep convection to overshoot the tropopause (Xian and Fu, 2015; Shi et al., 2017). The tropopause-penetrating convection generates warming in the upper troposphere and cooling near the lapse-rate tropopause and in the lower stratosphere.

The development of indices to predict occurrences of convection has always been a challenge for atmospheric research. Santhi et al. (2014) compared stability indices estimated from RO and radiosonde profiles, with particular focus on the Convective Available Potential Energy (CAPE). A high correlation between the RO and radiosonde estimates of

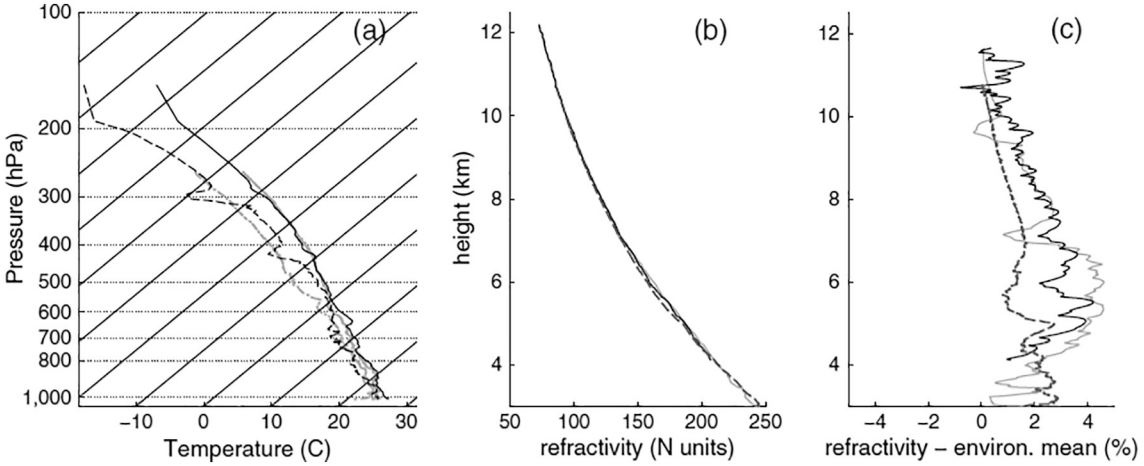

Fig. 12. Profiles of temperature and refractivity on 13 September 2010 in tropical depression (pre-Hurricane Karl) south of Jamaica. (a) Temperature (solid) and dewpoint (dashed) profiles from dropsonde (black) and radiosonde (gray). (b) refractivity from RO (black), radiosonde (dashed) and dropsonde (gray). (c) Difference of refractivity from environmental mean of RO (black), radiosonde (dashed) and dropsonde (gray). (Source: Fig. 6 from Murphy et al., 2015).

all the indices demonstrated that RO could be effectively used to assess the probability of thunderstorms in maritime areas where radiosondes are usually not available. However, the errors in using RO increase when the profiles do not reach the lowest layers of the troposphere.

The PRE-Depression Investigation of Cloud systems in the Tropics (PREDICT) used an airborne GNSS receiver to collect a large number of RO soundings in the vicinity of developing tropical depressions (Murphy et al., 2015). Despite the difficulties of obtaining RO profiles from an airborne receiver, the campaign obtained 21 refractivity profiles of high quality when compared with co-located dropsondes and the ERA-Interim re-analyses (Fig. 12).

A large number of thermodynamic profiles, especially in the area of the developing convection, would very likely improve the forecasts of intensity and location of the storms. An OSSE study assimilating 2.5 million simulated RO profiles in the WRF model (Leidner et al., 2017) has shown the capability of RO to make a better forecast of deep convection, largely through improving the analysis of the lower tropospheric moisture analysis.

4.2.3. Tropical cyclones

The application of GNSS RO to the study of TC has demonstrated the importance of RO observations in the tropics, particularly in improving the lower and middle tropospheric WV analysis.

4.2.3.1. TC and bending angle profiles. The high vertical resolution of RO and the insensitivity to clouds and precipitation make RO a powerful tool for observing the internal structure of the TC, and the sensitivity of the bending angle has been exploited to retrieve accurate information on the TC structure.

Biondi et al. (2011a) demonstrated for the first time that GNSS RO could be used to analyze the TC structure using bending angles. They studied two specific cases, Hurricane Bertha 2008 and Typhoon Hondo 2008, comparing the observed bending angle profile with its climatological value in the same area. The analysis of a relatively small number of COSMIC RO profiles co-located with the TC tracks (8 for Bertha and 7 for Hondo) showed a large bending angle anomaly corresponding to the TC cloud top height. Generalizing the study with a statistically relevant number of co-locations (1194) coming from 5 different missions (GPS-MET, CHAMP, SAC-C, COSMIC and GRACE), Biondi et al. (2011b) showed that the TCs are characterized by a positive bending angle anomaly in the UTLS corresponding to the TC cloud top height. A validation of the cloud top height from RO with observations of the Cloud-Aerosol Lidar with Orthogonal Polarization (CALIOP) onboard CALIPSO and radiosondes showed a RMSE of 365 m (Biondi et al., 2013).

Recently, Lasota et al. (2018) selected 50 ROs co-located with CloudSat measurements to study the sensitivity of the RO bending angle to the clouds in TC. In agreement with previous studies, they found a significant impact of the clouds on the bending angle profile with a clear signature detectable between 8 and 15 km of height.

4.2.3.2. TC and profiles of temperature and water vapor. Each ocean basin is characterized by different TC cloud top altitudes (Biondi et al., 2015) with higher altitudes and colder cloud tops in the Southern Hemisphere. More than 15,000 co-locations from all available RO missions were selected within a radius of 600 km from the TC eye in the period 2001–2014 and binned into ocean basins, hemispheres, and tropics/extra-tropics to compare the cloud top heights with the climatological tropopause to evaluate overshooting conditions. Fig. 13 shows an example of RO temperature anomalies in the North Atlantic. The warm anomalies in the middle and upper troposphere are well known, since at least the study by Jordan and Jordan (1954), and are caused by the release of latent heat in the TC convection. The cold anomalies above the warm anomalies in the lower stratosphere, are also well known since the study by Koteswaram (1967), and are caused by

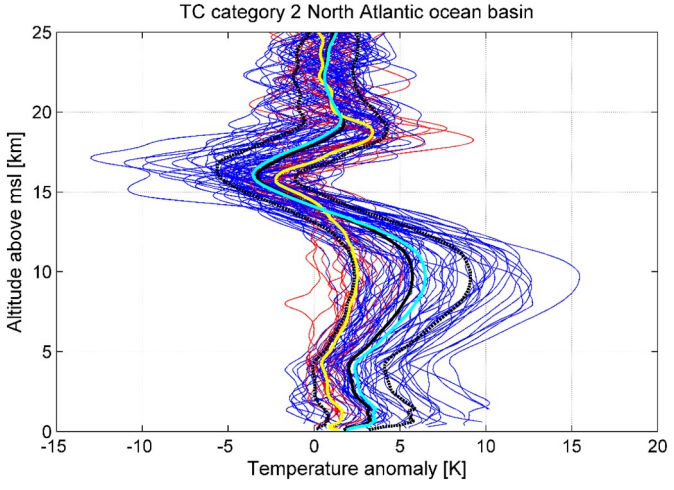

Fig. 13. RO temperature anomaly profiles during TC category 2 in the North Atlantic Ocean basin. Tropical profiles (red), extratropical profiles (blue), mean tropical (yellow), mean extratropical (light blue), mean of all profiles and ± standard deviation (black). (Source: Fig. 5 from Biondi et al., 2015). (For interpretation of the references to colour in this figure legend, the reader is referred to the web version of this article.)

overshooting convective tops and adiabatic lifting above the convection. The warm anomalies situated above the cold anomalies and centered at about 18 km have not been well observed or explained because of the lack of radiosonde and aircraft observations at this altitude and the thinness of the layer, making observations by microwave and infrared sounders difficult. The results showed that overshooting occurs more frequently in the Southern Hemisphere and in the Northern Indian ocean, confirming the finding of Romps and Kuang (2009) using infrared satellite imagery.

Winterbottom and Xiao (2010) compared RO temperature and WV profiles with radiosondes and global analyses in TC during the period 1995–2006 and concluded that the RO quality was high enough and the horizontal footprint small enough to study mesoscale phenomena. Anthes et al. (2008) and Anthes (2011) showed examples of temperature and WV profiles from RO soundings for typhoon Toraji 2001, and the positive effect of their assimilation in WRF model for hurricane Ernesto 2006.

Biondi et al., 2013 and Rivoire et al. (2016) used RO temperature profiles to find cooling at the TC cloud top height. This capability was confirmed by independent analyses (e.g. Davis et al., 2014), and was also useful in training other satellite sensors to retrieve the TC warm core (Zou and Tian, 2018). The cloud top cooling often results in a double tropopause in TC (Biondi et al., 2011b; Biondi et al., 2013; Vergados et al., 2014). Ravindra Babu et al. (2015) and Venkat Ratnam et al. (2016b) analyzed the impact of different TC on the UTLS and the tropopause structure by using CHAMP and COSMIC RO observations in the Bay of Bengal and the Arabian Sea. They computed the Cold Point Tropopause (CPT), the Lapse Rate Tropopause (LRT) and the TTL climatological values and the observed values during TC with profiles radially distributed around the cyclone eye. They also computed the variation of the tropopause height according to the TC structure and intensity. Results showed a decrease of TTL thickness due to the combined effect of lower CPT and higher convective tropopause. An increase of WV in the lower stratosphere has been observed from 500 to 1000 km away from the TC center (Venkat Ratnam et al., 2016b) and in the UT corresponding to the TC eyewall (Vergados et al., 2013).

4.2.3.3. TC and gravity waves. Intense convective towers in TC usually generate gravity waves that transport energy from the lower to upper atmosphere. As gravity waves propagate upward, they influence the atmospheric general circulation. Applying suitable processing, such as fast Fourier transforms, wavelet transforms, and image-processing tools, spectral characteristics of GW from RO vertical perturbation profiles can be extracted (Chane Ming et al., 2014). Using these profiles, Chane Ming et al. (2014) observed GW in the lower stratosphere, associated with the TC Ivan 2008 intensification phase in the northwestern Indian Ocean. In general, RO data reveal strong GW activity associated with TC, with the source located below the tropopause and with an increased potential energy in the lower stratosphere before and during the cyclone activity as shown in Fig. 14 and Fig. 15 (Rakshit et al., 2018).

4.2.3.4. Impact of RO on TC forecasts. The assimilation of RO refractivity observations in NWP models has shown a significant positive impact on many TC forecasts. Many studies focused on single events such as Hurricane Ernesto (Liu et al., 2012), Super-cyclone Gonu 2007 (Huang et al., 2010; Anisetty et al., 2014), Typhoon Usagi 2007 (Kunii et al., 2012), Typhoons Sinlaku 2008, Hagupit 2008 and Jangmi 2008 (Hsiao et al., 2012), Typhoons Megi 2010 and Haiyan 2013 (Chen et al., 2018b), and Tropical Cyclone Phailin 2013 (Hima Bindu et al., 2016). In addition, Chen et al. (2018a) showed a positive impact of assimilating airborne RO profiles in Hurricane Karl 2010 during the PREDICT campaign.

Chen et al. (2015) analyzed a complete TC season and found a modest, but statistically significant improvement in track forecasts when RO observations were used (Fig. 16). Most studies show an improvement of the intensity and track forecast by assimilating RO refractivities, especially in areas where conventional observations are rare. In some specific cases the RO data resulted in a significant error reduction for WV and wind forecasts compared to dropsonde and radiosondes.

4.2.4. Atmospheric rivers

Neiman et al. (2008) published the first analysis of AR based on GNSS RO. They selected 66 RO profiles within a strong AR impacting the US West Coast in November 2006 and showed that the thermodynamic and moisture structures revealed by these profiles were consistent with the same structures obtained with dropsondes, satellite images and re-analyses. Ma et al. (2011), as a sequel to Neiman et al. (2008) assessed the impact of the assimilation of COSMIC and CHAMP RO profiles in the WRF model on the analysis and prediction of this AR. In this detailed analysis they used 370 COSMIC profiles and 63 CHAMP profiles, concluding that the use of RO profiles improved the water vapor analysis for the AR. Eiserloh and Chiao (2015) simulated four strong ARs that affected the US West Coast over a short time in winter 2012 and showed that assimilating RO profiles in the WRF model produced better forecasts of AR than those without RO.

5. GNSS reflectometry

GNSS-Reflectometry (GNSS-R) is a technique that exploits GNSS signals after reflection off the Earth surface, acting like a bistatic radar. Transmitted navigation signals are forward scattered off the surface, and dedicated GNSS-R receivers on land, airborne, or spaceborne platforms detect and correlate the reflected signals with direct ones to retrieve geophysical information about the reflecting surface (Zavorotny et al., 2014). Typical detected surface properties include ocean roughness and sea surface height, tsunami detection (Stosius et al., 2010), storm surges (Peng et al., 2019), soil moisture, vegetation, snow depth, sea ice extent, and ocean surface wind speed (Foti et al., 2015). The latter property can be used to improve the tropical cyclones intensity forecast.

On December 15, 2016, NASA launched the Cyclone Global Navigation Satellite System (CYGNSS) mission. CYGNSS uses eight LEO micro-satellites for the measurements of ocean surface winds in and near the eye of tropical cyclones (https://directory.eoportal.org/web/eoportal/satellite-missions/c-missions/cygnss). Each satellite receives both direct GPS signals and reflected ones from the ocean surface, enabling frequent observations of the investigated region (Ruf et al., 2019). The mission aims to improve cyclone forecasting by a better insight of the air dynamics near the storm core, providing a large amount of observations useful for the understanding and modeling of the inner core of the cyclones. Fig. 17 shows measurements of wind speed measurements by CYGNSS of Typhoon Trami in September 2018 (Ruf et al., 2018).

6. Limitations and future directions

This review has highlighted how GNSS GB and RO observations have had a positive impact on extreme weather and climate science and predictions. High precision and accuracy, high vertical resolution, and all-weather capability are key-points for the “GNSS Meteorology” success. However, GB and RO observations have limitations as well as new potential applications, which will be addressed by future research.

6.1. GNSS GB

Global coverage and high temporal and horizontal resolution of atmospheric WV is a high priority for improving severe weather predictions. Currently the global network of GNSS GB products is sparse, especially over the oceans. The network could be improved with additional receivers installed over land and on islands, ships and buoys in

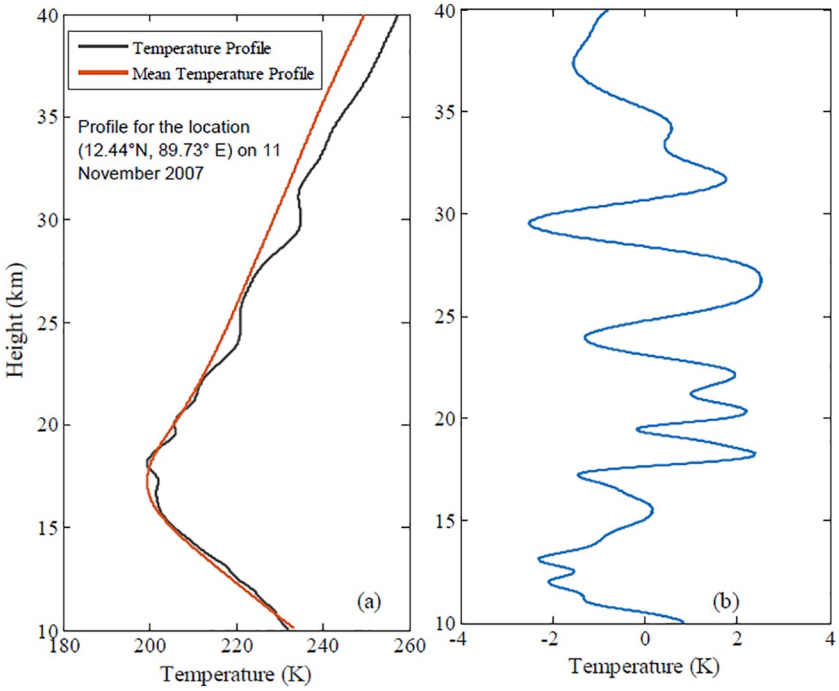

Fig. 14. (a) Radio occultation temperature (black) and mean temperature profile (red) and (b) perturbation profile during the tropical cyclone Sidr for the location (12.44°N, 89.73° E) on 11 November 2007. (Source: Fig. 1 from Rakshit et al., 2018). (For interpretation of the references to colour in this figure legend, the reader is referred to the web version of this article.)

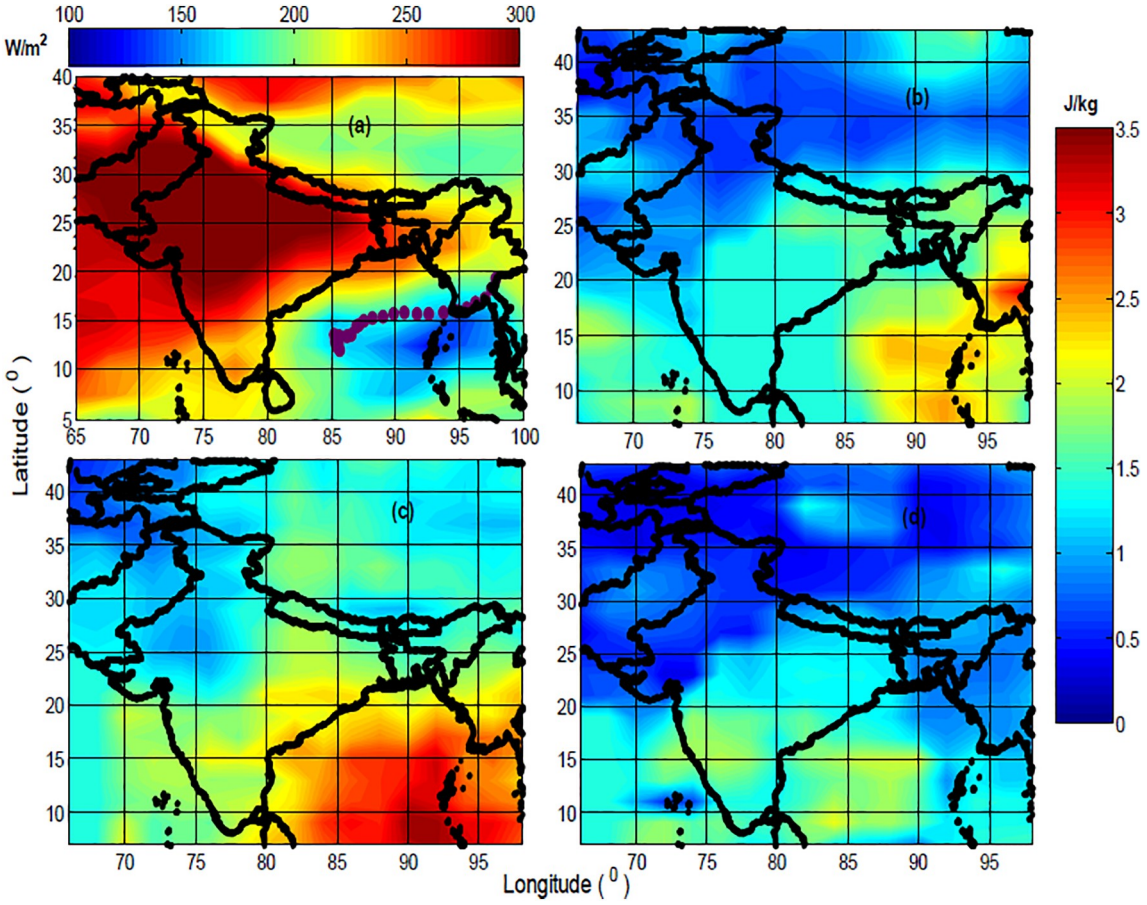

Fig. 15. (a) Path of Cyclone Nargis superimposed on the average outgoing longwave radiation (W/m^2) value during 27 April-03 May 2008. Contour plots of average potential energy (J/kg) in the height range 19–26 km: (b) before the storm (18–26 April), (c) during the storm (27 April − 03 May), and (d) after the storm (8–16 May 2008). (Source: Fig. 3 from Rakshit et al., 2018).

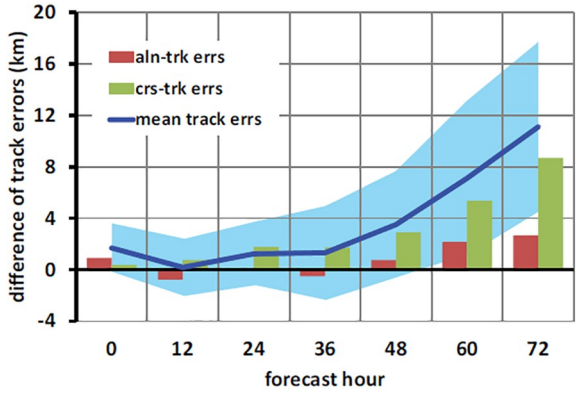

Fig. 16. Difference between mean track errors, along track errors, and cross-track errors of forecasts without and with RO observations. (Source: Fig. 5 from Chen et al., 2015).

the oceans.

The observed behavior of IWV during extreme events is often restricted to isolated cases and therefore may not be indicative of general patterns. It is necessary to analyze additional events to draw general conclusions and provide thresholds or dynamic indicators useful to detect and predict them.

High-resolution and short-range NWP models require humidity measurements more detailed than those currently available, chiefly to predict small-scale convective phenomena. Multi-GNSS (GPS, GLONASS, Galileo and BeiDou) processing would increase the number of observations and improve the azimuth and elevation angle coverage (Guerova et al., 2016). Development of new multi-GNSS processing and product testing will be particularly useful and challenging for the observing and forecasting of extreme events.

Improvements in GNSS ground infrastructure and data processing, as well as product flow standardization, should lead to the availability of real-time accurate products from worldwide ground stations, boosting severe event research and applications in the future. Worldwide climatological studies can benefit from post-processing long time series of GNSS observations adopting a homogenization strategy, i.e. the same coherent analysis approach (Wang et al., 2007).

A number of on-going strategies and future synergies are currently under investigation in the GNSS meteorology community:

- Validation of GNSS slant delays using different software (Kačmařík et al., 2017)
- Validation of WV estimations by using independent ground-based instruments and sensors onboard satellite platforms (Bonafoni et al., 2013).
- Increase of the receiver density with low-cost sensors (Realini et al., 2015), for instance developing single frequency GNSS receivers (Krietemeyer et al., 2018).
- Improvement of GNSS tomography: since tomography combines signal delays from different directions to obtain 3D fields of the atmospheric WV, the quality of the tomographic reconstruction can be improved by increasing the density of GNSS stations and improving the inversion techniques. Further improvements due to the increased number of observations is expected when Galileo and BeiDou products are available (Guerova et al., 2016).
- Additional studies to better define, from GNSS products, thresholds and indicators of heavy rainfalls and deep convections, or more generally indices of atmospheric activity, for advanced forecasts.
- Additional studies exploiting the synergy of different instruments (radar, microwave radiometers, radiosonde, profilers) to better characterize the main parameters describing a specific event.
- Flagging of hydrometeor delays in GNSS signals by synergy between radar and GNSS monitoring.

6.2. GNSS RO

The uneven quality of RO observations in the lower part of the troposphere (0–5 km), where most of the WV resides, limits

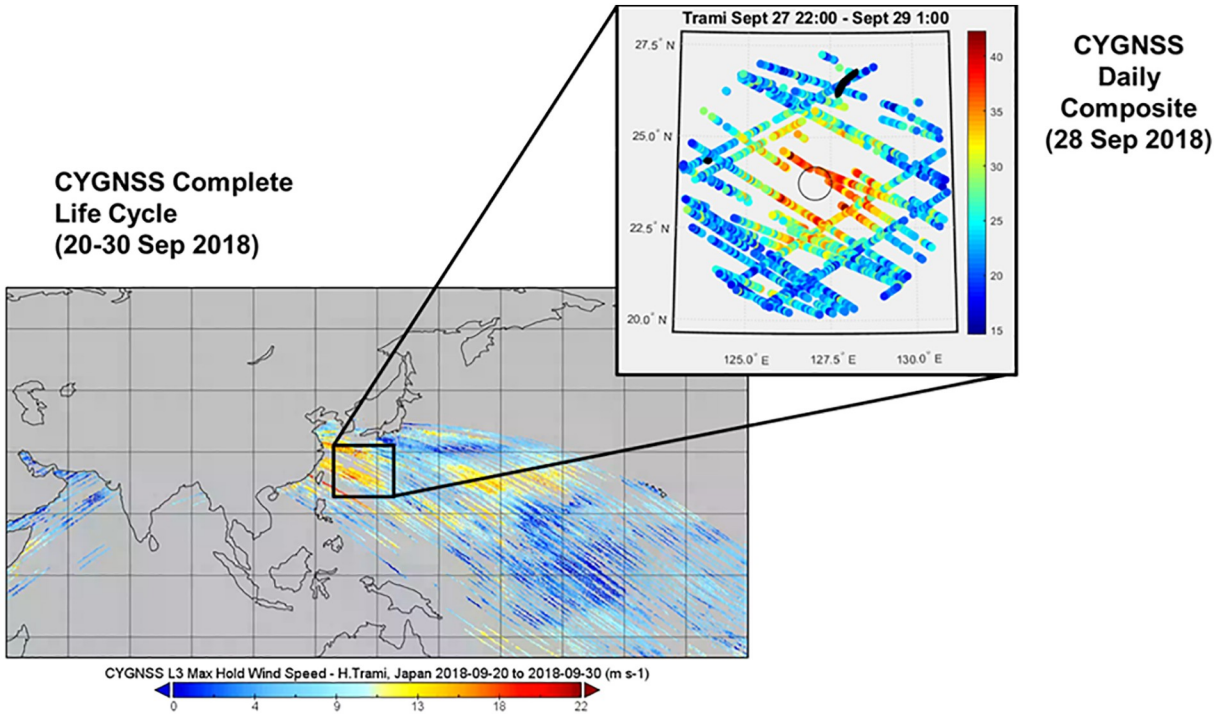

Fig. 17. CYGNSS wind speed measurements of Typhoon Trami in September 2018. Lower left image: composite over the period 20–30 September 2018 of all wind speed measurements. Upper right insert: measurements of 28 September re-gridded to a storm-centric coordinate system to highlight the wind speed structure in the inner core. (Source: Ruf et al., 2018).

atmospheric analysis and prediction of severe weather events, especially in the tropics. Although the excess phase delay is large in the moist lower troposphere, the signal amplitude can fall below the noise level due to defocusing and can undergo strong fluctuations, limiting the altitude range of RO reliability (Sokolovskiy et al., 2014). However, the many promising research results on specific cases show the value of high-quality RO soundings to retrieve WV in the lower troposphere (Burgos Fonseca et al., 2018) and make this a promising area for future improvement.

RO errors in the upper stratosphere are caused by ionospheric residuals after the dual-frequency ionospheric correction, bending angle initialization for Abel transform, and measurement noise (Kursinski et al., 1997). The impact of both large-scale and small-scale ionospheric residuals on profile retrievals changes under different solar activity conditions (Mannucci et al., 2011; Verkhoglyadova et al., 2015). Uncertainties in the Abel transform initialization cause a bias in the upper levels of refractivity profiles, since climatological background models used to derive the upper boundary conditions can introduce errors in the retrievals. These errors are difficult to evaluate since they depend on latitude and seasons (Steiner et al., 2013; Alexander et al., 2014; Scherllin-Pirscher et al., 2017).

Additional issues include the relatively small number of RO soundings per day compared to passive satellite sounding systems and the time to deliver observations to users (latency). Improvements in the spatial resolution and quality of GNSS RO products for severe event studies are planned. For instance, COSMIC-2, a new constellation of six LEO satellites launched on 25 June 2019 (https://www.cosmic.ucar.edu), promises to show a positive impact on research and prediction of tropical severe weather, especially TC. The COSMIC-2 constellation will collect more soundings due to the ability to track three navigation systems' signals (GPS, GLONASS, and Galileo) providing a significantly higher spatial and temporal density of RO profiles compared to previous missions. Furthermore, with the advanced GNSS RO payload, COSMIC-2 is expected to produce soundings with higher accuracy, increasing the impact of RO observations in extreme event monitoring and forecasts (https://directory.eoportal.org/web/eoportal/satellite-missions/content/-/article/formosat-7).

Identifying and reducing RO retrieval uncertainties in the lower tropical troposphere and refractivity biases due to super-refraction, which are frequently observed over oceans, are the main issues for tropical cyclone analysis and forecasts. To identify RO observations affected by super-refraction, a sufficiently high Signal-to-Noise ratio (SNR) is necessary (Sokolovskiy et al., 2014). This SNR requirement will be achievable with the advanced receiver system of the COSMIC-2 mission, allowing the analysis of TC with higher quality RO soundings. Furthermore, the six LEO satellites of COSMIC-2 will collect > 6000 RO soundings per day over the tropics and subtropics (35°N–35°S), a significant increase compared to the past and present availability. The data assimilation of RO observations in NWP models will benefit from the new mission, increasing weighting of the RO observations on the basis of their improved quality. Overall, COSMIC-2 will allow a better monitoring of the tropical and subtropical WV pattern, a key-element in the observation and prediction of TC and heavy rainfall.

Additional missions beyond COSMIC-2 are planned. China will be launching additional RO missions. EUMETSAT launched METOP-C, which carries a GNSS receiver, on 7 November 2018. Several private companies are planning launches of thousands of satellites carrying GNSS receivers, which could provide more than an order of magnitude of RO soundings globally if the quality of the data is adequate, business model is successful and data access and other issues can be resolved (https://spacenews.com/the-still-unrealized-promise-of-commercial-earth-science-data/ and https://aerospaceamerica.aiaa.org/features/proving-themselves/)

Finally, basic research in the GNSS RO field continues to advance at a high theoretical level, with studies on assessing or enhancing the accuracy and utility of RO observations in Earth's atmosphere (Gorbunov and Kirchengast, 2018; Wee and Kuo, 2014). It is important to continue this fundamental research to make further theoretical and modeling advances, especially by using the new mission data.

Acknowledgments

R. Biondi was supported by the University of Padova within the project Volcanic clouds dEtection and monitoring for Studying the erUption impact on climate and aVIatiOn (VESUVIO), funded by the Programme Supporting TAlent in ReSearch (STARS) @ University of Padova. This work is also a contribution from the the Solar-Terrestrial Centre of Excellence (http://www.stce.be), funded by the Belgian Federal Science Policy Office. Anthes was supported by NSF-NASA Grant AGS-1522830; the support of Eric DeWeaver and Jack Kaye is greatly appreciated.

References

Adams, D.K., Fernandes, R.M., Kursinski, E.R., Maia, J.M., Sapucci, L.F., Machado, L.A., Vitorello, I., Monico, J.F., Holub, K.L., Gutman, S.I., Filizola, N., Bennett, R.A., 2011. A dense GNSS meteorological network for observing deep convection in the Amazon. Atmos. Sci. Lett. 12, 207–212. https://doi.org/10.1002/asl.312.

Adams, D.K., Gutman, S.I., Holub, K.L., Pereira, D.S., 2013. GNSS observations of deep convective time-scales in the Amazon. Geophys. Res. Lett. 40 (11), 2818–2823. https://doi.org/10.1002/grl.50573.

Adams, D.K., Fernandes, R.M., Holub, K.L., Gutman, S.I., Barbosa, H.M., Machado, L.A., Calheiros, A.J.P., Bennett, R.A., Kursinski, E.R., Sapucci, L.F., DeMets, C., Chagas, G.F.B., Arellano, A., Filizola, N., Rocha, A.A.A., Silva, R.A., Assunção, L.M.F., Cirino, G.G., Pauliquevis, T., Portela, B.T.T., Sá, A., de Sousa, J.M., Tanaka, L.M.S., 2015. The Amazon dense GNSS meteorological network: a new approach for examining water vapor and deep convection interactions in the tropics. Bull. Amer. Met. Society 96 (12), 2151–2165. https://doi.org/10.1175/BAMS-D-13-00171.1.

Adams, D.K., Barbosa, H.M., Gaitán De Los Ríos, K.P., 2017. A spatiotemporal water vapor–deep convection correlation metric derived from the Amazon dense GNSS meteorological network. Mon. Weath. Rev. 145 (1), 279–288. https://doi.org/10.1175/MWR-D-16-0140.1.

Alexander, P., de la Torre, A., Llamedo, P., Hierro, R., 2014. Precision estimation in temperature and refractivity profiles retrieved by GPS radio occultations. J. Geophys. Res. 119, 8624–8638. https://doi.org/10.1002/2013JD021016.

Burgos Fonseca, Y., Alexander, P., de la Torre, A., Hierro, R., LLamedo, P., Calori, A., 2018. Comparison between GNSS ground-based and GPS radio occultation precipitable water observations over ocean-dominated regions. Atmos. Res. 209, 115–122. https://doi.org/10.1016/j.atmosres.2018.03.017.

Aniseti, S.K.A.V. Prasad Rao, Huang, C.Y., Chen, S.Y., 2014. Impact of FORMOSAT-3/COSMIC radio occultation data on the prediction of super cyclone Gonu (2007): a case study. Nat. Hazards 70 (2), 1209–1230. https://doi.org/10.1007/s11069-013-0870-0.

Anthes, R.A., 2011. Exploring Earth's atmosphere with radio occultation: contributions to weather, climate and space weather. Atmos. Meas. Tech. 4, 1077–1103. https://doi.org/10.5194/amt-4-1077-2011.

Anthes, R.A., Rocken, C., Kuo, Y.-H., 2000. Applications of COSMIC to meteorology and climate. In: Special issue of Terrestrial, Atmos. Ocean. Sci. (TAO). vol. 11. pp. 115–156. https://doi.org/10.3319/tao.2000.11.1.115(cosmic).

Anthes, R.A., Bernhardt, P.A., Chen, Y., Cucurull, L., Dymond, K.F., Ector, D., Healy, S.B., Ho, S., Hunt, D.C., Kuo, Y., Liu, H., Manning, K., McCormick, C., Meehan, T.K., Randel, W.J., Rocken, C., Schreiner, W.S., Sokolovskiy, S.V., Syndergaard, S., Thompson, D.C., Trenberth, K.E., Wee, T., Yen, N.L., Zeng, Z., 2008. The COSMIC/FORMOSAT-3 mission: early results. Bull. Amer. Meteor. Soc. 89, 313–334. https://doi.org/10.1175/BAMS-89-3-313.

Argus, D.F., Landerer, F.W., Wiese, D.N., Martens, H.R., Fu, Y., Famiglietti, J.S., ... Watkins, M.M., 2017. Sustained water loss in California's mountain ranges during severe drought from 2012 to 2015 inferred from GPS. J. Geophys. Res. 122, 10,559–10,585. https://doi.org/10.1002/2017JB014424.

Banacos, P.C., Schultz, D.M., 2005. The use of moisture flux convergence in forecasting convective initiation: historical and operational perspectives. Wea. Forecast. 20, 351–366. https://doi.org/10.1175/WAF858.1.

Barindelli, S., Realini, E., Venuti, G., Fermi, A., Gatti, A., 2018. Detection of water vapor time variations associated with heavy rain in northern Italy by geodetic and low-cost GNSS receivers. Earth, Planets and Space 70 (1), 28.

Bauer, H.S., Wulfmeyer, V., Schwitalla, T., Zus, F., Grzeschik, M., 2011. Operational assimilation of GPS slant path delay measurements into the MM5 4D-VAR system. Tellus a: dyn. Meteor. Ocean. 63 (2), 263–282. https://doi.org/10.1111/j.1600-0870.2010.00489.x.

Benevides, P., Catalao, J., Nico, G., 2019. Neural network approach to forecast hourly intense rainfall using gnss precipitable water vapor and meteorological sensors. Remote Sens. 11, 966. https://doi.org/10.3390/rs11080966.

Bevis, M., Businger, S., Herring, T.A., Rocken, C., Anthes, R.A., Ware, R.H., 1992. GPS meteorology: remote sensing of atmospheric water vapour using the Global Positioning System. J. Geophys. Res. 97 (D14), 15787–15801. https://doi.org/10.1029/92JD01517.

Bevis, M., Businger, S., Chiswell, S., Herring, T.A., Anthes, R.A., Rocken, C., Ware, R.H., 1994. GPS meteorology: mapping zenith wet delays onto precipitable water. J. Appl. Meteorol. 33, 379–386. https://doi.org/10.1175/1520-0450(1994)033<0379:GMMZWD>2.0.CO;2.

Biondi, R., Neubert, T., Syndergaard, S., Nielsen, J., 2011a. Measurements of the upper troposphere and lower stratosphere during tropical cyclones using the GPS radio occultation technique. Adv. Space Res. 47 (2). https://doi.org/10.1016/j.asr.2010.05.031.

Biondi, R., Neubert, T., Syndergaard, S., Nielsen, J.K., 2011b. Radio occultation bending angle anomalies during tropical cyclones. Atmos. Meas. Tech. 4 (6), 1053–1060. https://doi.org/10.5194/amt-4-1053-2011.

Biondi, R., Randel, W.J., Ho, S.P., Neubert, T., Syndergaard, S., 2012. Thermal structure of intense convective clouds derived from GPS radio occultations. Atmos. Chem. Phys. 12 (12), 5309–5318. https://doi.org/10.5194/acp-12-5309-2012.

Biondi, R., Ho, S.P., Randel, W., Syndergaard, S., Neubert, T., 2013. Tropical cyclone cloud-top height and vertical temperature structure detection using GPS radio occultation measurements. J. Geophys. Res. Atmos. 118 (11), 5247–5259. https://doi.org/10.1002/jgrd.50448.

Biondi, R., Steiner, A.K., Kirchengast, G., Rieckh, T., 2015. Characterization of thermal structure and conditions for overshooting of tropical and extratropical cyclones with GPS radio occultation. Atmos. Chem. Phys. 15 (9), 5181–5193. https://doi.org/10.5194/acp-15-5181-2015.

Blewitt, G., 1989. Carrier phase ambiguity resolution for the global positioning system applied to geodetic baselines up to 2000 km. J. Geophys. Res. 94, 10187–10203. https://doi.org/10.1029/JB094iB08p10187.

Bonafoni, S., Biondi, R., 2016. The usefulness of the Global Navigation Satellite Systems (GNSS) in the analysis of precipitation events. Atmos. Res. 167, 15–23. https://doi.org/10.1016/j.atmosres.2015.07.011.

Bonafoni, S., Mattioli, V., 2018. Tropospheric dry delay for microwaves using a model based on surface measurements on a global scale. IET Microw. Ant. Propag. (1751-8725) 12 (1), 9–14. https://doi.org/10.1049/iet-map.2016.1148.

Bonafoni, S., Mazzoni, A., Cimini, N., Montopoli, M., Pierdicca, N., Basili, P., Ciotti, P., Carlesimo, G., 2013. Assessment of water vapor retrievals from a GPS receiver network. GPS Solutions 17 (4), 475–484. https://doi.org/10.1007/s10291-012-0293-5.

Boniface, K., Ducrocq, V., Jaubert, G., Yan, X., Brousseau, P., Masson, F., Champollion, C., Chéry, J., Doerflinger, E., 2009. Impact of high-resolution data assimilation of GPS zenith delay on Mediterranean heavy rainfall forecasting. Ann. Geophys. 27, 2739–2753. https://doi.org/10.5194/angeo-27-2739-2009.

Borsa, A.A., Agnew, D.C., Cayan, D.R., 2014. Ongoing drought-induced uplift in the western United States. Science 345 (6204), 1587–1590. https://doi.org/10.1126/science.1260279.

Brenot, H., Ducrocq, V., Walpersdorf, A., Champollion, C., Caumont, O., 2006. GPS zenith delay sensitivity evaluated from high-resolution numerical weather prediction simulations of the 8–9 September 2002 flash flood over southeastern France. J. Geophys. Res. 111 (D15105). https://doi.org/10.1029/2004JD005726.

Brenot, H., Neméghaire, J., Delobbe, L., Clerbaux, N., De Meutter, P., Deckmyn, A., Delcloo, A., Frappez, L., Van Roozendael, M., 2013. Preliminary signs of the initiation of deep convection by GNSS. Atmos. Chem. Phys. 13 (11), 5425–5449. https://doi.org/10.5194/acp-13-5425-2013.

Brenot, H., Walpersdorf, A., Reverdy, M., Van Baelen, J., Ducrocq, V., Champollion, C., Masson, F., Doerflinger, E., Collard, P., Giroux, P., 2014. A GPS network for tropospheric tomography in the framework of the Mediterranean hydrometeorological observatory Cévennes-Vivarais (South-Eastern France). Atmos. Meas. Tech (7), 553–578. https://doi.org/10.5194/amt-7-553-2014.

Brenot, H., Rohm, W., Kačmařík, M., Möller, G., Sá, A., Tondaś, D., Rapant, L., Biondi, R., Manning, T., Champollion, C., 2018. Cross-validation of GPS tomography models and methodological improvements using CORS network. Atmos. Meas. Tech. Discuss. https://doi.org/10.5194/amt-2018-292.

Calori, A., Santos, J.R., Blanco, M., Pessano, H., Llamedo, P., Alexander, P., de la Torre, A., 2016. Ground-based GNSS network and integrated water vapor mapping during the development of severe storms at the Cuyo region (Argentina). Atmos. Res. 176, 267–275. https://doi.org/10.1016/j.atmosres.2016.03.002.

Cardellach, E., Tomás, S., Oliveras, S., Padullés, R., Rius, A., de La Torre-Juárez, M., Turk, F.J., Ao, C.O., Kursinski, E.R., Schreiner, B., Ector, D., Cucurull, L., 2015. Sensitivity of PAZ LEO polarimetric GNSS radio-occultation experiment to precipitation events. IEEE Trans. Geosci. Remote Sens. 53 (1), 190–206. https://doi.org/10.1109/TGRS.2014.2320309.

Cardellach, E., Padullés, R., Tomás, S., Turk, F.J., Ao, C.O., de la Torre-Juárez, M., 2018. Probability of intense precipitation from polarimetric GNSS radio occultation observations. Q.J.R. Meteor.Soc. 144 (1), 206–220. https://doi.org/10.1002/qj.3161.

Cardellach, E., Oliveras, S., Rius, A., Tomás, S., Ao, C.O., Franklin, G.W., Iijima, B.A., Kuang, D., Meehan, T.K., Padullés, R., de la Torre-Juarez, M., Turk, F.J., Hunt, D., Schreiner, W.S., Sokolovskiy, S.V., Van Hove, T., Weiss, J.P., Yoon, Y., Zeng, Z., Clapp, J., Xia-Serafino, W., Cerezo, F., 2019. Sensing heavy precipitation with GNSS polarimetric radio occultations. Geophys. Res. Lett. https://doi.org/10.1029/2018GL080412.

Champollion, C., Masson, F., Van Baelen, J., Walpersdorf, A., Chéry, J., Doerflinger, E., 2004. GPS monitoring of the tropospheric water vapor distribution and variation during the 9 September 2002 torrential precipitation episode in the Cévennes (southern France). J. Geophys. Res. 109 (D24). https://doi.org/10.1029/2004JD004897.

Champollion, C., Flamant, C., Bock, O., Masson, F., Turner, D.D., Weckwerth, T., 2009. Mesoscale GPS tomography applied to the 12 June 2002 convective initiation event of IHOP_2002. Q.J.R. Meteor.Soc. 135 (640), 645–662. https://doi.org/10.1002/qj.386.

Chane Ming, F., Ibrahim, C., Barthe, C., Jolivet, S., Keckhut, P., Liou, Y.-A., Kuleshov, Y., 2014. Observation and a numerical study of gravity waves during tropical cyclone Ivan (2008). Atmos. Chem. Phys. 14, 641–658. https://doi.org/10.5194/acp-14-641-2014.

Chen, Y.C., Hsieh, M.E., Hsiao, L.F., Kuo, Y.H., Yang, M.J., Huang, C.Y., Lee, C.S., 2015. Systematic evaluation of the impacts of GPSRO data on the prediction of typhoons over the northwestern Pacific in 2008-2010. Atmos. Meas. Tech. 8 (6), 2531–2542. https://doi.org/10.5194/amt-8-2531-2015.

Chen, B., Liu, Z., Wong, W., Woo, W., 2017. Detecting water vapor variability during heavy precipitation events in hong kong using the gps tomographic technique. J. Atmos. Ocean. Technol. 34, 1001–1019. https://doi.org/10.1175/JTECH-D-16-0115.1.

Chen, X.M., Chen, S.H., Haase, J.S., Murphy, B.J., Wang, K.N., Garrison, J.L., Chen, S.Y., Huang, C.Y., Adhikari, L., Xie, F., 2018a. The impact of airborne radio occultation observations on the simulation of hurricane karl (2010). Mon. Weather Rev. 146 (1), 329–350. https://doi.org/10.1175/MWR-D-17-0001.1.

Chen, S.Y., Zhao, H., Huang, C.Y., 2018b. Impacts of GNSS Radio Occultation Data on Predictions of Two Super-Intense Typhoons with WRF Hybrid Variational-Ensemble Data Assimilation. J. Aeronaut. Astronaut. Aviat. 50 (4), 347–364.

Chew, C.C., Small, E.E., 2014. Terrestrial water storage response to the 2012 drought estimated from GPS vertical position anomalies. Geophys. Res. Lett. 41, 6145–6151. https://doi.org/10.1002/2014GL061206.

Choy, S., Wang, C., Zhang, K., Kuleshov, Y., 2013. GPS sensing of precipitable water vapour during the March 2010 Melbourne storm. Adv. Space Res. 52 (9), 1688–1699. https://doi.org/10.1016/j.asr.2013.08.004.

Cucurull, L., Vandenberghe, F., Barker, D., Vilaclara, E., Rius, A., 2004. Three-dimensional variational data assimilation of ground-based GPS ZTD and meteorological observations during the 14 December 2001 storm event over the western Mediterranean Sea. Mon. Weather Rev. 132 (3), 749–763. https://doi.org/10.1175/1520-0493(2004)132<0749:TVDAOG>2.0.CO;2.

Davis, C.A., Ahijevych, D.A., Haggerty, J.A., Mahoney, M.J., 2014. Observations of temperature in the upper troposphere and lower stratosphere of tropical weather disturbances. J. Atmos. Sci. 71 (5), 1593–1608. https://doi.org/10.1175/JAS-D-13-0278.1.

de Haan, S., Holleman, I., Holtslag, A.A., 2009. Real-time water vapor maps from a GPS surface network: construction, validation, and applications. J. Appl. Meteorol. Climatol. 48 (7), 1302–1316. https://doi.org/10.1175/2008JAMC2024.1.

de la Torre, A., Hierro, R., Llamedo, P., Rolla, A., Alexander, P., 2011. Severe hailstorms near Southern Andes in the presence of mountain waves. Atmos. Res. 101 (1–2), 112–123. https://doi.org/10.1016/j.atmosres.2011.01.015.

de la Torre-Juárez, M., Padullés, R., Turk, F.J., Cardellach, E., 2018. Signatures of heavy precipitation on the thermodynamics of clouds seen from satellite: changes observed in temperature lapse rates and missed by weather analyses. J. Geophys. Res. 123 (23), 13,033–13,045. https://doi.org/10.1029/2017JD028170.

De Pondeca, M.S., Zou, X., 2001. A case study of the variational assimilation of GPS zenith delay observations into a mesoscale model. J. Appl. Meteorol. 40 (9), 1559–1576. https://doi.org/10.1175/1520-0450(2001)040<1559:ACSOTV>2.0.CO;2.

Eiserloh, A.J., Chiao, S., 2015. Modeling studies of landfalling atmospheric rivers and orographic precipitation over northern California. Meteorog. Atmos. Phys. 127 (1), 1–16. https://doi.org/10.1007/s00703-014-0350-4.

Ferreira, V.G., Montecino, H.C., Ndehedehe, C.E., Heck, B., Gong, Z., de Freitas, S.R.C., Westerhaus, M., 2018. Space-based observations of crustal deflections for drought characterization in Brazil. Sci. Total Environ. 644, 256–273. https://doi.org/10.1016/j.scitotenv.2018.06.277.

Foti, G., Gommenginger, C., Jales, P., Unwin, M., Shaw, A., Robertson, C., Roselló, J., 2015. Spaceborne GNSS reflectometry for ocean winds: first results from the UK TechDemoSat-1 mission. Geophys. Res. Lett. 42 (13), 5435–5441. https://doi.org/10.1002/2015GL064204.

Fu, Y., Argus, D.F., Landerer, F.W., 2015. GPS as an independent measurement to estimate terrestrial water storage variations in Washington and Oregon. J. Geophys. Res. 120, 552–566. https://doi.org/10.1002/2014JB011415.

Gorbunov, M.E., Kirchengast, G., 2018. Wave-optics uncertainty propagation and regression-based bias model in GNSS radio occultation bending angle retrievals. Atmos. Meas. Tech. 11, 111–125. https://doi.org/10.5194/amt-11-111-2018.

Gorbunov, M.E., Benzon, H.H., Jensen, A.S., Lohmann, M.S., Nielsen, A.S., 2004. Comparative analysis of radio occultation processing approaches based on Fourier integral operators. Radio Sci. 39 (6). https://doi.org/10.1029/2003RS002916.

Graham, E., Koffi, E.N., Mätzler, C., 2012. An observational study of air and water vapour convergence over the Bernese Alps, Switzerland, during summertime and the development of isolated thunderstorms. Meteorol. Z. 21 (6), 561–574. https://doi.org/10.1127/0941-2948/2012/0347.

Guerova, G., Simeonov, T., Yordanova, N., 2014. The sofia university atmospheric data archive (SUADA). Atmos. Meas. Tech. 7, 2683–2694. https://doi.org/10.5194/amt-7-2683-2014.

Guerova, G., Jones, J., Douša, J., Dick, G., de Haan, S., Pottiaux, E., Bock, O., Pacione, R., Elgered, G., Vedel, H., Bender, M., 2016. Review of the state of the art and future prospects of the ground-based GNSS meteorology in Europe. Atmos. Meas. Tech. 9, 5385–5406. https://doi.org/10.5194/amt-9-5385-2016.

Guo, Y.R., Kuo, Y.H., Dudhia, J., Parsons, D., Rocken, C., 2000. Four-dimensional variational data assimilation of heterogeneous mesoscale observations for a strong convective case. Mon. Weather Rev. 128 (3), 619–643. https://doi.org/10.1175/1520-0493(2000)128<0619:FDVDAO>2.0.CO;2.

Ha, S.Y., Kuo, Y.H., Guo, Y.R., Rocken, C., Van Hove, T., 2002. Comparison of GPS slant wet delay measurements with model simulations during the passage of a squall line. Geophys. Res. Lett. 29 (23). https://doi.org/10.1029/2002GL015891.

Ha, J.H., Lim, G.H., Choi, S.J., 2014. Assimilation of GPS radio occultation refractivity data with WRF 3D-VAR and its impact on the prediction of a heavy rainfall event. J.

Appl. Meteorol. Climatol. 53 (6), 1381–1398. https://doi.org/10.1175/JAMC-D-13-0224.1.
Hierro, R., Steiner, A.K., de la Torre, A., Alexander, P., Llamedo, P., 2018. Orographic and convective gravity waves above the Alps and andes mountains during GPS radio occultation events–a case study. Atmos. Meas. Tech. 11, 3523–3539. https://doi.org/10.5194/amt-11-3523-2018.
Hima Bindu, H., Venkat Ratnam, M., Yesubabu, V., Narayana Rao, T., Kesarkar, A., Naidu, C.V., 2016. Characteristics of cyclone generated gravity waves observed using assimilated WRF model simulations over Bay of Bengal. Atmos. Res. 180, 178–188. https://doi.org/10.1016/j.atmosres.2016.05.021.
Ho, S.-P., Anthes, R.A., Ao, C.O., Healy, S., Horanyi, A., Hunt, D., Mannucci, A.J., Pedatella, N., Randel, W.J., Simmons, A., Steiner, A., Xie, F., Yue, X., Zeng, Z., 2019. The COSMIC-FORMOSAT-3 radio occultation mission after 12 years: accomplishments, remaining challenges, and potential impacts of COSMIC-2. Bull. Am. Meteorol. Soc. 100, 2019 (in review).
Hsiao, L.-F., Chen, D.-S., Kuo, Y.-H., Guo, Y.-R., Yeh, T.-C., Hong, J.-S., Fong, C.-Z., Lee, C.-S., 2012. Application of WRF 3D-VAR to operational typhoon prediction in Taiwan: impact of outer loop and partial cycling approaches. Weath. Forecast. 27 (5), 1249–1263. https://doi.org/10.1175/WAF-D-11-00131.1.
Huang, C.Y., Kuo, Y.H., Chen, S.Y., et al., 2010. Impact of GPS radio occultation data assimilation on regional weather predictions. GPS Solutions 14, 35. https://doi.org/10.1007/s10291-009-0144-1.
Huang, C.-Y., Chen, S.-Y., Rao Anisetty, S.K.A.V.P., Yang, S.-C., Hsiao, L.-F., 2016. An impact study of Gps radio occultation observations on frontal rainfall prediction with a local bending angle operator. Weath. Forecast. 31 (1), 129–150. https://doi.org/10.1175/WAF-D-15-0085.1.
Huelsing, H.K., Wang, J., Mears, C., Braun, J.J., 2017. Precipitable water characteristics during the 2013 Colorado flood using ground-based GPS measurements. Atmos. Meas. Tech. 10, 4055–4066. https://doi.org/10.5194/amt-10-4055-2017.
Iwabuchi, T., Naito, I., Mannoji, N., 2000. A comparison of Global Positioning System retrieved precipitable water vapor with the numerical weather prediction analysis data over the Japanese Islands. J. Geophys. Res. 105 (D4), 4573–4585. https://doi.org/10.1029/1999JD901007.
Iwabuchi, T., Miyazaki, S.I., Heki, K., Naito, I., Hatanaka, Y., 2003. An impact of estimating tropospheric delay gradients on tropospheric delay estimations in the summer using the Japanese nationwide GPS array. J. Geophys. Res. 108 (D10). https://doi.org/10.1029/2002JD002214.
Jiang, W., Yuan, P., Chen, H., Cai, J., Li, Z., Chao, N., Sneeuw, N., 2017. Annual variations of monsoon and drought detected by GPS: a case study in Yunnan. China. Sci. Rep. 7, 5874. https://doi.org/10.1038/s41598-017-06095-1.
Jin, S., Zhang, T., 2016. Terrestrial water storage anomalies associated with drought in southwestern USA from GPS observations. Surv. Geophys. 37, 1139. https://doi.org/10.1007/s10712-016-9385-z.
Johnston, B.R., Xie, F., Liu, C., 2018. The effects of deep convection on regional temperature structure in the tropical upper troposphere and lower stratosphere. J. Geophys. Res. 123 (3), 1585–1603. https://doi.org/10.1002/2017JD027120.
Jordan, C.L., Jordan, E.S., 1954. On the mean thermal structure of tropical cyclones. J. Meteorol. 11, 440–448. https://doi.org/10.1175/1520-0469(1954)011<0440:OTMTSO>2.0.CO;2.
Kačmařík, M., Douša, J., Dick, G., Zus, F., Brenot, H., Möller, G., Pottiaux, E., Kapłon, J., Hordyniec, P., Václavovic, P., Morel, L., 2017. Inter-technique validation of tropospheric slant total delays. Atmos. Meas. Tech. 10, 2183–2208. https://doi.org/10.5194/amt-10-2183-2017.
Kawabata, T., Iwai, H., Seko, H., Shoji, Y., Saito, K., Ishii, S., Mizutani, K., 2014. Cloud-resolving 4D-Var assimilation of Doppler wind lidar data on a meso-gamma-scale convective system. Mon. Weather Rev. 142 (12), 4484–4498. https://doi.org/10.1175/MWR-D-13-00362.1.
Khaykin, S.M., Pommereau, J.P., Hauchecorne, A., 2013. Impact of land convection on temperature diurnal variation in the tropical lower stratosphere inferred from COSMIC GPS radio occultations. Atmos. Chem. Phys. 13 (13), 6391–6402. https://doi.org/10.5194/acp-13-6391-2013.
Kingsmill, D.E., Neiman, P.J., Moore, B.J., Hughes, M., Yuter, S.E., Ralph, F.M., 2013. Kinematic and thermodynamic structures of Sierra barrier jets and overrunning atmospheric rivers during a landfalling winter storm in northern California. Mon. Weather Rev. 141, 2015–2036. https://doi.org/10.1175/MWR-D-12-00277.1.
Klobuchar, J.A., 1996. In: Parkinson, B.W., Spilker Jr.J.J. (Eds.), Ionospheric effects on GPS. Global Positioning System: Theory and Applications. Chapter 12. AIAA, Washington.
Koteswaram, P., 1967. On the structure of hurricanes in the upper troposphere and lower stratosphere. Mon. Weather Rev. 95 (8), 541–564. https://doi.org/10.1175/1520-0493(1967)095<0541:OTSOHI>2.3.CO;2.
Krietemeyer, A., ten Veldhuis, M.C., van der Marel, H., Realini, E., van de Giesen, N., 2018. Potential of cost-efficient single frequency GNSS receivers for water vapor monitoring. Remote Sens. 10 (9), 1493. https://doi.org/10.3390/rs10091493.
Kunii, M., Seko, H., Ueno, M., Shoji, Y., Tsuda, T., 2012. Impact of assimilation of gps radio occultation refractivity on the forecast of typhoon usagi in 2007. J. Met. Soc. Japan 90 (2), 255–273. https://doi.org/10.2151/jmsj.2012-207.
Kursinski, E.R., Hajj, G.A., Schofield, J.T., Linfield, R.P., Hardy, K.R., 1997. Observing Earth's atmosphere with radio occultation measurements using the Global Positioning System. J. Geophys. Res. 112 (D19), 23,429–23,465. https://doi.org/10.1029/97JD01569.
Lasota, E., Rohm, W., Liu, C.-Y., Hordyniec, P., 2018. Cloud detection from radio occultation measurements in tropical cyclones. Atmosphere 9 (11), 418. https://doi.org/10.3390/atmos9110418.
Leidner, S.M., Nehrkorn, T., Henderson, J., Mountain, M., Yunck, T., Hoffman, R.N., 2017. A severe weather quick observing system simulation experiment (Quickosse) of global navigation satellite system (GNSS) radio occultation (RO) superconstellations. Mon. Weather Rev. 145 (2), 637–651. https://doi.org/10.1053/ejso.2002.1307.
Li, G., Deng, J., 2013. Atmospheric water monitoring by using ground-based GPS during heavy rains produced by TPV and SWV. Adv. Meteorol. 2013 (793957), 12. https://doi.org/10.1155/2013/793957.
Lichten, S.M., Border, J.S., 1987. Strategies for high-precision global positioning system orbit determination. J. Geophys. Res. 92 (B12), 12751–12762. https://doi.org/10.1029/JB092iB12p12751.
Lindskog, M., Ridal, M., Thorsteinsson, S., Ning, T., 2017. Data assimilation of GNSS zenith total delays from a nordic processing centre. Atmos. Chem. Phys. 17 (22), 13983–13998. https://doi.org/10.5194/acp-17-13983-2017.
Liou, Y.-A., Huang, C.-Y., 2000. GPS observations of PW during the passage of a typhoon. Earth Planet. Space 52, 709–712. https://doi.org/10.1186/BF03352269.
Liu, H., Anderson, J., Kuo, Y.-H., 2012. Improved analyses and forecasts of hurricane ernesto's genesis using radio occultation data in an ensemble filter assimilation system. Mon. Weather Rev. 140 (1), 151–166. https://doi.org/10.1175/MWR-D-11-00024.1.
Ma, Z., Kuo, Y.-H., Ralph, F.M., Neiman, P.J., Wick, G.A., Sukovich, E., Wang, B., 2011. Assimilation of GPS radio occultation data for an intense atmospheric river with the NCEP regional GSI system. Mon. Weather Rev. 139 (7), 2170–2183. https://doi.org/10.1175/2011MWR3342.1.
Manning, T., Zhang, K., Rohm, W., Choy, S., Hurter, F., 2012. Detecting severe weather in Australia using GPS tomography. J. Glob. Posit. Syst. 11 (1), 58–70. https://doi.org/10.5081/jgps.11.1.58.
Mannucci, A.J., Ao, C.O., Pi, X., Iijima, B.A., 2011. The impact of large scale ionospheric structure on radio occultation retrievals. Atmos. Meas. Tech. 4, 2837–2850. https://doi.org/10.5194/amt-4-2837-2011.
Masoumi, S., McClusky, S., Koulali, A., Tregoning, P., 2017. A directional model of tropospheric horizontal gradients in Global Positioning System and its application for particular weather scenarios. J. Geophys. Res. 122 (8), 4401–4425. https://doi.org/10.1002/2016JD026184.
McPhillips, L.E., Chang, H., Chester, M.V., Depietri, Y., Friedman, E., Grimm, N.B., Kominoski, J.S., McPhearson, T., Méndez-Lázaro, P., Rosi, E.J., Shafiei Shiva, J., 2018. Defining extreme events: a cross-disciplinary review. Earth's Fut. 6, 441–455. https://doi.org/10.1002/2017EF000686.
Melbourne, W., Davis, E., Duncan, C., Hajj, G., Hardy, K., Kursinski, E., Meehan, T., Young, L., Yunck, T., 1994. The application of space borne GPS to atmospheric limb sounding and global change monitoring. JPL Publ. 94-18, 147.
Mircheva, B., Tsekov, M., Meyer, U., Guergana, Guerova G., 2017. Anomalies of hydrological cycle components during the 2007 heat wave in Bulgaria. J. Atmos. Solar-Terr. Phys. 165–166, 1–9. https://doi.org/10.1016/j.jastp.2017.10.005.
Moker Jr., J.M., Castro, C.L., Arellano Jr., A.F., Serra, Y.L., Adams, D.K., 2018. Convective-permitting hindcast simulations during the North American Monsoon GPS transect experiment 2013: establishing baseline model performance without data assimilation. J. Appl. Meteorol. Climatol. 57 (8), 1683–1710. https://doi.org/10.1175/JAMC-D-17-0136.1.
Moore, A.W., Small, I.J., Gutman, S.I., Bock, Y., Dumas, J.L., Fang, P., Haase, J.S., Jackson, M.E., Laber, J.L., 2015. National weather service forecasters use GPS precipitable water vapor for enhanced situational awareness during the Southern California summer monsoon. Bull. Amer. Met. Society 96 (11), 1867–1877. https://doi.org/10.1175/BAMS-D-14-00095.1.
Murphy, B.J., Haase, J.S., Muradyan, P., Garrison, J.L., Wang, K.N., 2015. Airborne GPS radio occultation refractivity profiles observed in tropical storm environments. J. Geophys. Res. 120 (5), 1690–1709. https://doi.org/10.1002/2014JD022931.
Neiman, P.J., Ralph, F.M., Wick, G.A., Kuo, Y.-H., Wee, T.-K., Ma, Z., Taylor, G.H., Dettinger, M.D., 2008. Diagnosis of an intense atmospheric river impacting the pacific northwest: storm summary and offshore vertical structure observed with COSMIC satellite retrievals. Mon. Weather Rev. 136 (11), 4398–4420. https://doi.org/10.1175/2008MWR2550.1.
Neiman, P.J., Hughes, M., Moore, B.J., Ralph, F.M., Sukovich, E.M., 2013. Sierra barrier jets, atmospheric rivers, and precipitation characteristics in northern california: a composite perspective based on a Network of wind profilers. Mon. Weather Rev. 141, 4211–4233. https://doi.org/10.1175/MWR-D-13-00112.1.
Neiman, P.J., Ralph, F.M., Moore, B.J., Zamora, R.J., 2014. The regional influence of an intense sierra barrier jet and landfalling atmospheric river on orographic precipitation in northern California: a case study. J. Hydrometeorol. 15, 1419–1439. https://doi.org/10.1175/JHM-D-13-0183.1.
Neiman, P.J., Moore, B.J., White, A.B., Wick, G.A., Aikins, J., Jackson, D.L., Spackman, J.R., Ralph, F.M., 2016. An airborne and ground-based study of a long-lived and intense atmospheric river with mesoscale frontal waves impacting California during CalWater-2014. Mon. Weather Rev. 144, 1115–1144. https://doi.org/10.1175/MWR-D-15-0319.1.
Padullés, R., Cardellach, E., Wang, K.N., Ao, C.O., Joseph Turk, F., de La Torre-Juárez, M., 2018. Assessment of global navigation satellite system (GNSS) radio occultation refractivity under heavy precipitation. Atmos. Chem. Phys. 18 (16), 11697–11708. https://doi.org/10.5194/acp-18-11697-2018.
Paulik, L.C., Birner, T., 2012. Quantifying the deep convective temperature signal within the tropical tropopause layer (TTL). Atmos. Chem. Phys. 12 (24), 12183–12195. https://doi.org/10.5194/acp-12-12183-2012.
Peng, S.Q., Zou, X., 2004. Impact on short-range precipitation forecasts from assimilation of ground-based GPS zenith total delay and rain gauge precipitation observations. J. Met. Soc. Japan. Ser. II 82 (1B), 491–506. https://doi.org/10.2151/jmsj.2004.491.
Peng, D., Hill, E.M., Li, L., Switzer, A.D., Larson, K.M., 2019. Application of GNSS interferometric reflectometry for detecting storm surges. GPS Sol. 23 (2), 47.
Poli, P., Moll, P., Rabier, F., Desroziers, G., Chapnik, B., Berre, L., Healy, S.B., Andersson, E., El Guelai, F.-Z., 2007. Forecast impact studies of zenith total delay data from

European near real-time GPS stations in Meteo France 4D-VAR. J. Geophys. Res. 112, D06114. https://doi.org/10.1029/2006JD007430.
Priego, E., Jones, J., Porres, M.J., Seco, A., 2017. Monitoring water vapour with GNSS during a heavy rainfall event in the Spanish mediterranean area. Geomatics, Nat. Hazards Risk 8 (2), 282–294. https://doi.org/10.1080/19475705.2016.1201150.
Rakshit, G., Jana, S., Maitra, A., 2018. Gravity wave behavior in lower stratosphere during tropical cyclones over the bay of bengal. Radio Sci. 53 (11), 1356–1367. https://doi.org/10.1029/2018RS006614.
Ralph, F.M., Neiman, P.J., Kiladis, G.N., Weickmann, K., Reynolds, D.W., 2011. A multiscale observational case study of a pacific atmospheric river exhibiting tropical–extratropical connections and a mesoscale frontal wave. Mon. Weather Rev. 139, 1169–1189. https://doi.org/10.1175/2010MWR3596.1.
Ravindra Babu, S., Venkat Ratnam, M., Basha, G., Krishnamurthy, B.V., Venkateswararao, B., 2015. Effect of tropical cyclones on the tropical tropopause parameters observed using COSMIC GPS RO data. Atmos. Chem. Phys. 15 (18), 10239–10249. https://doi.org/10.5194/acp-15-10239-2015.
Realini, E., Sato, K., Tsuda, T., Oigawa, M., Iwaki, Y., Shoji, Y., Seko, H., 2015. Local-scale precipitable water vapor retrieval from high-elevation slant tropospheric delays using a dense network of GNSS receivers. In: Rizos, C., Willis, P. (Eds.), IAG 150 Years. International Association of Geodesy Symposia. vol. 143. Springer, Cham, pp. 485–490.
Rivoire, L., Birner, T., Knaff, J.A., 2016. Evolution of the upper-level thermal structure in tropical cyclones. Geophys. Res. Lett. 43 (19), 10,530–10,537. https://doi.org/10.1002/2016GL070622.
Rohm, W., Yuan, Y., Biadeglgne, B., Zhang, K., Le Marshall, J., 2014. Ground-based GNSS ZTD/IWV estimation system for numerical weather prediction in challenging weather conditions. Atmos. Res. 138, 414–426. https://doi.org/10.1016/j.atmosres.2013.11.026.
Rohm, W., Guzikowski, J., Wilgan, K., Kryza, M., 2019. 4D-VAR assimilation of GNSS zenith path delays and precipitable water into a numerical weather prediction model WRF. Atmos. Meas. Tech. 12 (1), 345–361. https://doi.org/10.5194/amt-12-345-2019.
Romps, D.M., Kuang, Z., 2009. Overshooting convection in tropical cyclones. Geophys. Res. Lett. 36, L09804. https://doi.org/10.1029/2009GL037396.
Ruf, C., Gleason, S., McKague, D.S., Posselt, D.J., Moghaddam, M., 2018. The NASA CYGNSS SmallSat Constellation. AGU Annual Meeting 2018, Paper NH24A-01. (Washington, DC).
Ruf, C., Cardellach, E., Clarizia, M.P., Galdi, C., Gleason, S.T., Paloscia, S., 2019. Foreword to the special issue on cyclone global navigation satellite system (CYGNSS) early on orbit performance. IEEE J. Sel. Top. Appl. Earth Obs. Remote Sens. 12 (1), 3–6. https://doi.org/10.1109/JSTARS.2018.2885391.
Saastamoinen, J., 1972. Atmospheric correction for the troposphere and stratosphere in radio ranging of satellites. In: Henriksen, S.W. (Ed.), Geophys Monogr Ser. vol. 15. pp. 247–251. https://doi.org/10.1029/GM015p0247.
Santhi, Y.D., Ratnam, M.V., Dhaka, S.K., Rao, S.V., 2014. Global morphology of convection indices observed using COSMIC GPS RO satellite measurements. Atmos. Res. 137, 205–215. https://doi.org/10.1016/j.atmosres.2013.10.002.
Sapucci, L.F., Machado, L.A., de Souza, E.M., Campos, T.B., 2018. Global positioning system precipitable water vapour (GPS-PWV) jumps before intense rain events: a potential application to nowcasting. Met. Applicat. 26 (1), 49–63. https://doi.org/10.1002/met.1735.
Scherllin-Pirscher, B., Steiner, A.K., Kirchengast, G., Schwaerz, M., Leroy, S.S., 2017. The power of vertical geolocation of atmospheric profiles from GNSS radio occultation. J. Geophys. Res. Atmos. 122. https://doi.org/10.1002/2016JD025902.
Seco, A., González, P.J., Ramírez, F., García, R., Prieto, E., Yagüe, Fernández, J., 2009. GPS monitoring of the tropical storm delta along the Canary Islands track. November 28–29, 2005. Pure Appl. Geophys 166, 1519–1531. https://doi.org/10.1007/s00024-009-0502-5.
Seko, H., Shimada, S., Nakamura, H., Kato, T., 2000. Three-dimensional distribution of water vapor estimated from tropospheric delay of GPS data in a mesoscale precipitation system of the Baiu front. Earth, Plan. Space 52 (11), 927–933. https://doi.org/10.1186/BF03352307.
Seko, H., Nakamura, H., Shoji, Y., Iwabuchi, T., 2004. The meso-γ scale water vapor distribution associated with a thunderstorm calculated from a dense network of GPS receivers. J. Met. Soc. Japan. Ser. II 82 (1B), 569–586. https://doi.org/10.2151/jmsj.2004.569.
Serra, Y.L., Adams, D.K., Minjarez-Sosa, C., Moker Jr., J.M., Arellano, A.F., Castro, C.L., Quintanar, A.I., Alatorre, L., Granados, A., Esteban Vasquez, G., Holub, K., De Mets, C., 2016. The North American monsoon GPS transect experiment 2013. Bull. Amer. Met. Soc 97 (11), 2103–2115. https://doi.org/10.1175/BAMS-D-14-00250.1.
Sharifi, M.A., Khaniani, A.S., Joghataei, M., 2015. Comparison of GPS precipitable water vapor and meteorological parameters during rainfalls in Tehran. Meteorog. Atmos. Phys. 127 (6), 701–710. https://doi.org/10.1007/s00703-015-0383-3.
Shi, C., Cai, W., Guo, D., 2017. Composition and thermal structure of the upper troposphere and lower stratosphere in a penetrating mesoscale convective complex determined by satellite observations and model simulations. Adv. Meteorol. 2017, 6404796. https://doi.org/10.1155/2017/6404796.
Shoji, Y., Yamauchi, H., Mashiko, W., Sato, E., 2014. Estimation of local-scale precipitable water vapor distribution around each GNSS station using slant path delay. SOLA 10, 29–33. https://doi.org/10.2151/sola.2014-007.
Shoji, Y., Mashiko, W., Yamauchi, H., Sato, E., 2015. Estimation of local-scale precipitable water vapor distribution around each GNSS station using slant path delay: evaluation of a severe tornado case using high-resolution NHM. SOLA 11, 31–35. https://doi.org/10.2151/sola.2015-008.
Smith, E.K., Weintraub, S., 1953. The constants in the equation for atmospheric refractive index at radio frequencies. Proc. Inst. Radio Eng. 41, 1035–1037. https://doi.org/10.1109/JRPROC.1953.274297.
Sokolovskiy, S., Schreiner, W., Zeng, Z., Hunt, D., Lin, Y.-C., Kuo, Y.-H., 2014. Observation, analysis, and modeling of deep radio occultation signals: effects of tropospheric ducts and interfering signals. Radio Sci. 49, 954–970. https://doi.org/10.1002/2014RS005436.
Solheim, F.S., Vivekanandan, J., Ware, R.H., Rocken, C., 1999. Propagation delays induced in GPS signals by dry air, water vapor, hydrometeors, and other particulates. J. Geophys. Res. 104, 9663–9670. https://doi.org/10.1029/1999JD900095.
Song, D.-S., Grejner-Brzezinska, D.A., 2009. Remote sensing of atmospheric water vapor variation from GPS measurements during a severe weather event. Earth Planet. Space 61, 1117–1125. https://doi.org/10.1186/BF03352964.
Steiner, A.K., Hunt, D., Ho, S.-P., Kirchengast, G., Mannucci, A.J., Scherllin-Pirscher, B., Gleisner, H., von Engeln, A., Schmidt, T., Ao, C., Leroy, S.S., Kursinski, E.R., Foelsche, U., Gorbunov, M., Heise, S., Kuo, Y.-H., Lauritsen, K.B., Marquardt, C., Rocken, C., Schreiner, W., Sokolovskiy, S., Syndergaard, S., Wickert, J., 2013. Quantification of structural uncertainty in climate data records from GPS radio occultation. Atmos. Chem. Phys. 13, 1469–1484. https://doi.org/10.5194/acp-13-1469-2013.
Stosius, R., Beyerle, G., Hoechner, A., Wickert, J., Lauterjung, J., 2010. The impact on tsunami detection from space using GNSS-reflectometry when combining GPS with GLONASS and Galileo on GNSS-Reflectometry tsunami detection from space. Adv. Space Res. 47 (5), 843–853. https://doi.org/10.1016/j.asr.2010.09.022. 201.
Terradellas, E., Téllez, B., 2010. The use of products from ground-based GNSS observations in meteorological nowcasting. Adv. Geosci. 26, 77–82. https://doi.org/10.5194/adgeo-26-77-2010.
Teunissen, P., Kleusberg, A., Bock, Y., Beutler, G., Weber, R., Langley, R.B., van der Marel, Hans, Blewitt, G., Gload, C.C., Colombo, O.L., 1998. GPS for Geodesy, 2nd ed. Springerhttps://doi.org/10.1007/978-3-642-72011-6.
Van Baelen, J., Penide, G., 2009. Study of water vapor vertical variability and possible cloud formation with a small network of GPS stations. Geophys. Res. Lett. 36 (2). https://doi.org/10.1029/2008GL036148.
Van Baelen, J., Reverdy, M., Tridon, F., Labbouz, L., Dick, G., Bender, M., Hagen, M., 2011. On the relationship between water vapour field evolution and the life cycle of precipitation systems. Q.J.R. Meteor.Soc. 137 (S1), 204–223. https://doi.org/10.1002/qj.785.
Vedel, H., Huang, X.Y., Haase, J., Ge, M., Calais, E., 2004. Impact of GPS zenith tropospheric delay data on precipitation forecasts in Mediterranean France and Spain. Geophys. Res. Lett. 31 (2). https://doi.org/10.1029/2003GL017715.
Venkat Ratnam, D., Sri Sai Chaithanya, K., Ramalingeswara Reddy, M., Yamini, M.M., Sridhar, M., 2016a. GPS water vapour content variations during heat wave occurred during May, 2015, over South Indian Region. ARPN J. Engin. App. Sci. 11 (17), 10460–10463.
Venkat Ratnam, M., Ravindra Babu, S., Das, S.S., Basha, G., Krishnamurthy, B.V., Venkateswararao, B., 2016b. Effect of tropical cyclones on the stratosphere-troposphere exchange observed using satellite observations over the North Indian Ocean. Atmos. Chem. Phys. 16 (13), 8581–8591. https://doi.org/10.5194/acp-16-8581-2016.
Vergados, P., Mannucci, A.J., Su, H., 2013. A validation study for GPS radio occultation data with moist thermodynamic structure of tropical cyclones. J. Geophys. Res. 118 (16), 9401–9413. https://doi.org/10.1002/jgrd.50698.
Vergados, P., Johnny Luo, Z., Emanuel, K., Mannucci, A.J., 2014. Observational tests of hurricane intensity estimations using GPS radio occultations. J. Geophys. Res. 119 (4), 1936–1948. https://doi.org/10.1002/2013JD020934.
Verkhoglyadova, O.P., Mannucci, A.J., Ao, C.O., Iijima, B.A., Kursinski, E.R., 2015. Effect of small-scale ionospheric variability on GNSS radio occultation data quality. J. Geophys. Res. 120, 7937–7951. https://doi.org/10.1002/2015JA021055.
Wang, J., Zhang, L., Dai, A., Van Hove, T., Van Baelen, J., 2007. A near-global 2-hourly data set of atmospheric precipitable water from ground-based GPS measurements. J. Geophys. Res. 112, D11107. https://doi.org/10.1029/2006JD007529.
Wang, H., He, J., Wei, M., Zhang, Z., 2015. Synthesis analysis of one severe convection precipitation event in Jiangsu using ground-based GPS technology. Atmos. 6 (7), 908–927. https://doi.org/10.3390/atmos6070908.
Wang, M., Wang, J., Bock, Y., Liang, H., Dong, D., Fang, P., 2019. Dynamic Mapping of the Movement of Landfalling Atmospheric Rivers over Southern California with GPS Data. Geophys. Res. Lett. 46 (6), 3551–3559.
Ware, R., Exner, M., Feng, D., Gorbunov, M., Hardy, K., Herman, B., Kuo, Y., Meehan, T., Melbourne, W., Rocken, C., Schreiner, W., Sokolovskiy, S., Solheim, F., Zou, X., Anthes, R., Businger, S., Trenberth, K., 1996. GPS sounding of the atmosphere from low earth orbit: preliminary results. Bull. Amer. Meteor. Soc. 77, 19–40. https://doi.org/10.1175/1520-0477.
Wee, T.-K., Kuo, Y.-H., 2014. A perspective on the fundamental quality of GPS radio occultation data. Atmos. Meas. Tech. Discuss. 7, 9481–9508. https://doi.org/10.5194/amtd-7-9481-2014.
Winterbottom, H.R., Xiao, Q., 2010. An intercomparison of GPS RO retrievals with co-located analysis and in situ observations within tropical cyclones. Adv. Meteorol. 2010, 1–10. https://doi.org/10.1155/2010/715749.
Xian, T., Fu, Y., 2015. Characteristics of tropopause-penetrating convection determined by TRMM and COSMIC GPS radio occultation measurements. J. Geophys. Res. 120 (14), 7006–7024. https://doi.org/10.1002/2014JD022633.
Xiong, Z., Zhang, B., Yao, Y., 2019. Comparisons between the WRF data assimilation and the GNSS tomography technique in retrieving 3-D wet refractivity fields in Hong Kong. Ann. Geophys. 37 (1), 25–36. https://doi.org/10.5194/angeo-37-25-2019.
Yan, X., Ducrocq, V., Poli, P., Hakam, M., Jaubert, G., Walpersdorf, A., 2009a. Impact of GPS zenith delay assimilation on convective-scale prediction of Mediterranean heavy rainfall. J. Geophys. Res. 114 (D3). https://doi.org/10.1029/2008JD011036.
Yan, X., Ducrocq, V., Jaubert, G., Brousseau, P., Poli, P., Champollion, C., Flamant, C., Boniface, K., 2009b. The benefit of GPS zenith delay assimilation to high-resolution

quantitative precipitation forecasts: a case-study from COPS IOP 9. Q.J.R. Meteor.Soc. 135 (644), 1788–1800. https://doi.org/10.1002/qj.508.
Yang, S.-C., Chen, S.-H., Chen, S.-Y., Huang, C.-Y., Chen, C.-S., 2014. Evaluating the impact of the COSMIC RO bending angle data on predicting the heavy precipitation episode on 16 June 2008 during SoWMEX-IOP8. Mon. Weather Rev. 142 (11), 4139–4163. https://doi.org/10.1175/MWR-D-13-00275.1.
Zavorotny, V., Gleason, S., Cardellach, E., Camps, A., 2014. Tutorial on remote sensing using GNSS bistatic radar of opportunity. IEEE Trans. Geosci. Remote Sens. 2 (4), 8–45. https://doi.org/10.1109/36.841977.
Zeng, Z., Sokolovskiy, S., Schreiner, W.S., Hunt, D., 2019. Representation of vertical structures by radio occultation observations in the upper troposphere and lower stratosphere: Comparison to high-resolution radiosonde profiles. J. Atmos. and Oceanic Tech. https://doi.org/10.1175/JTECH-D-18-0105.1. April 2019.
Zhang, M., Ni, Y., Zhang, F., 2007. Variational assimilation of GPS precipitable water vapor and hourly rainfall observations for a meso-β scale heavy precipitation event during the 2002 mei-yu season. Adv. Atmos. Sci. 24 (3), 509–526. https://doi.org/10.1007/s00376-007-0509-8.
Zhang, K., Manning, T., Wu, S., Rohm, W., Silcock, D., Choy, S., 2015. Capturing the signature of severe weather events in Australia using GPS measurements. IEEE J. Sel. Top. Appl. Earth Obs. Remote Sens. 8 (4), 1839–1847. https://doi.org/10.1109/JSTARS.2015.2406313.
Zou, X., Tian, X., 2018. Hurricane warm-core retrievals from AMSU-A and remapped ATMS measurements with rain contamination eliminated. J. Geophys. Res. 123 (19), 10,815–10,829. https://doi.org/10.1029/2018JD028934.